

Estimation of In-cylinder Trapped Gas Mass and Composition

Sepideh Nikkar

Master of Science Thesis in Mechanical Engineering
Estimation of In-cylinder Trapped Gas Mass and Composition

Sepideh Nikkar

LiTH-ISY-EX--17/5073--SE

Supervisor: **Ph.D. Andreas Thomasson**

ISY, Linköpings universitet

Ph.D. Erik Höckerdal

Scania CV AB

Examiner: **Prof. Lars Eriksson**

ISY, Linköpings universitet

*Division of Vehicular Systems
Department of Electrical Engineering
Linköping University
SE-581 83 Linköping, Sweden*

Copyright © 2017 Sepideh Nikkar

Upphovsrätt

Detta dokument hålls tillgängligt på Internet – eller dess framtida ersättare – från publiceringsdatum under förutsättning att inga extraordinära omständigheter uppstår.

Tillgång till dokumentet innebär tillstånd för var och en att läsa, ladda ner, skriva ut enstaka kopior för enskilt bruk och att använda det oförändrat för ick-eckommersiell forskning och för undervisning. Överföring av upphovsrätten vid en senare tidpunkt kan inte upphäva detta tillstånd. All annan användning av dokumentet kräver upphovsmannens medgivande. För att garantera äktheten, säkerheten och tillgängligheten finns lösningar av teknisk och administrativ art.

Upphovsmannens ideella rätt innefattar rätt att bli nämnd som upphovsman i den omfattning som god sed kräver vid användning av dokumentet på ovan beskrivna sätt samt skydd mot att dokumentet ändras eller presenteras i sådan form eller i sådant sammanhang som är kränkande för upphovsmannens litterära eller konstnärliga anseende eller egenart.

För ytterligare information om Linköping University Electronic Press se förlagets hemsida <http://www.ep.liu.se/>.

Copyright

The publishers will keep this document online on the Internet – or its possible replacement – from the date of publication barring exceptional circumstances.

The online availability of the document implies permanent permission for anyone to read, to download, or to print out single copies for his/her own use and to use it unchanged for non-commercial research and educational purpose. Subsequent transfers of copyright cannot revoke this permission. All other uses of the document are conditional upon the consent of the copyright owner. The publisher has taken technical and administrative measures to assure authenticity, security and accessibility.

According to intellectual property law the author has the right to be mentioned when his/her work is accessed as described above and to be protected against infringement.

For additional information about the Linköping University Electronic Press and its procedures for publication and for assurance of document integrity, please refer to its www home page: <http://www.ep.liu.se/>.

To my family

Abstract

To meet the constantly restricting emission regulations and develop better strategies for engine control systems, thorough knowledge of engine behavior is crucial. One of the characteristics to evaluate engine performance and its capability for power generation is in-cylinder pressure. Indeed, most of the diagnosis and control signals can be obtained by recording the cylinder pressure trace and predicting the thermodynamic variables [3].

This study investigates the correlation between the in-cylinder pressure and total trapped gas mass [10] with the main focus on estimating the in-cylinder gas mass as a part of a lab measuring procedure using the in-cylinder pressure sensors, or as a real-time method for implementation in an engine control unit that are not equipped with the cylinder pressure sensors. The motivation is that precise determination of air mass is essential for the fuel control system to convey the most-efficient combustion with lower emissions delivered to the after-treatment system [10].

For this purpose, a six-cylinder Diesel engine is used for recording the engine speed, engine torque, measuring the cylinder pressure profile resolved by the crank angle, intake and exhaust valve phasing as well as intake and exhaust manifold pressures and temperatures. Next, the most common ways of estimating the in-cylinder trapped gas mass are studied and the most reliable ones are investigated in-depth and a model with the acceptable accuracy in different operating conditions is proposed, explained and implemented. The model in has a thermodynamics basis and the relative errors is lower than $\pm 3\%$ in all the investigated tests. Afterwards, the most important findings are highlighted, the sources of errors are addressed and a sensitivity analysis is performed to evaluate the model robustness. Subsequently, method adjustment for other operating conditions is briefly explained, the potential future work is pointed and a complete set of results is presented in Appendix B.

Keywords: Diesel Engine, Cylinder Pressure, Residual Gas Mass, Gas Mass Composition, Cylinder Wall Temperature, Cylinder Pressure Correction

Acknowledgments

I would first like to express my deepest thanks of gratitude to my thesis examiner, Lars Eriksson, for introducing me to Scania, his useful comments and continuous support. I would also like to thank my thesis supervisors, Erik Höckerdal and Andreas Thomasson, very much for their expert advise, constant guidance and motivation during the entire master thesis and being patient with my questions and doubts without any hesitation. This study could not have been conducted successfully without their passionate supervision and consistent sharing of their experience and knowledge with me. Many sincere thanks to Martin Karlsson for granting me the opportunity to join his team as a master student and giving me a chance to develop myself in many different aspects.

My special thanks goes to my parents for their unconditional support, encouraging my activities, strengthening my enthusiasm and keeping me motivated. Last but not least, I would like to express my very profound gratitude my sister, Samira, and my brother-in-law, Vaheed, for their limitless support, being aside me always and giving me the right advice at the right time. My studies have become much more enjoyable with them.

Last but not least, I would also like to thank my friends who have made this journey more exciting to me.

Södertälje, June 2017
Sepideh Nikkar

Contents

List of Figures	xii
List of Tables	xiii
Notation	xv
1 Introduction	1
1.1 Background	1
1.2 Goal and Purpose	2
1.3 Thesis Outline	2
2 Internal Combustion Engines	5
2.1 Background	5
2.2 The Four Stroke Engine Cycle	6
2.3 Definitions	7
2.3.1 Valve Timing	7
2.3.2 Volumetric Efficiency	9
2.3.3 Residual Gas, EGR, Blow-By and Back-Flow	9
3 Research Study	11
3.1 Gas Mass Estimation	11
3.1.1 Standard Volumetric Efficiency Method	11
3.1.2 Δp Method	12
3.1.3 Correlation Method	14
3.1.4 Fitting Pressure Trace During Compression	15
3.1.5 Frequency Analysis of the Pressure Trace	16
3.1.6 Other Methods	17
3.2 Heat Transfer	17
3.2.1 Correlation for Time-Averaged Heat Flux	18
3.2.2 Correlation for Instantaneous Spatial-Averaged Heat Flux	19
3.2.3 Correlation for Instantaneous Local Heat Flux	20
3.3 Estimation of Cylinder Wall Temperature	20
3.3.1 First Method	20

3.3.2	Second Method	23
3.4	Summary	24
4	Method	25
4.1	Experimental Setup	25
4.2	Input Data	26
4.3	Pre-processing of in-cylinder pressure signals	27
4.3.1	The Need for Accurate Absolute Pressure Referencing	28
4.3.2	Pressure Offset	28
4.4	Assumptions	28
4.5	Chemical Reaction	29
4.6	Ideal Gas Constant, Specific Heat in Constant Pressure/Volume and Burned Gas Fraction	30
4.7	Residual Gas Mass	33
4.8	Heat Transfer Model	33
4.9	Total In-Cylinder Trapped Gas Mass	34
4.10	Cylinder Wall Temperature	36
4.11	Temperature at 70° BTDC	37
4.12	Cycles With Positive Valve Overlap	37
5	Results and Discussion	39
5.1	Experimental Data	41
5.2	Pressure Pegging	44
5.3	Total Gas, Fresh Air and Residual Gas Mass	45
5.4	Composition Fraction	47
5.5	Estimation of Temperatures	48
5.6	Pressure and Temperature Trace during Compression	50
5.7	Other Findings	52
5.7.1	Computational Costs	52
5.7.2	Optimization Process	54
5.7.3	Polytropic Index and Specific Heat Ratio	54
5.7.4	Temperature at 70° BTDC	57
6	Sensitivity Analysis	59
6.1	Intake and Exhaust Valve Closing Temperature	59
6.2	Cylinder Wall Temperature	62
6.3	Intake and Exhaust Valve Valve Lash	63
6.4	Pressure Pegging	64
6.5	Summary	65
7	Conclusions	67
8	Future Work	69
A	Another Alternative for Sensitivity of Air Mass to Intake and Exhaust Valve Closing Temperatures	71

Contents	xi
B A Complete Set of Results	73
Bibliography	87

List of Figures

2.1	The Four-Stroke Operating Cycle [12]	7
2.2	Valve Lifts and Cylinder Volume	8
3.1	Overall engine heat-transfer correlation for different types of IC engines [12]	18
3.2	Polytropic index and Specific Heat Ratio vs. Crank Angle [3]	22
3.3	Estimated polytropic index and Specific Heat Ratio vs. Crank Angle [3]	23
4.1	Experimental Setup	26
4.2	Overlap Factor [17]	38
5.1	Experimental Data and Demonstration of Pressure Trace, Indicator Diagram, Cylinder Volume and Valve Events for Test 2	42
5.2	Cylinder pressure trace for all the 12 Tests	43
5.3	Raw versus Corrected Cylinder Pressure Trace for Test 2	45
5.4	Measured and Predicted Pressure Curves during Compression for Test 2	51
5.5	Predicted Temperature Curve during Compression for Tests 1, 6, 9 and 12 From Left to Right, Top: test 1 and 6 Down: 9 and 12	52
5.6	Polytropic Index and specific heat ratio for Tests 2 and 6	55
5.7	Polytropic Index and specific heat ratio for Tests 9 and 12	56

List of Tables

3.1	C_1 and C_2 Coefficients for Woschni Correlation	20
4.1	Engine Geometry for Diesel Engine	26
4.2	Limit Values of the Experimental Data Set	27
5.1	A Complete Set of Tests	39
5.2	Other Experimental Data	40
5.3	Volume at the Opening and Closing of Intake and Exhaust Valves .	43
5.4	Pressure at the Opening and Closing of Intake and Exhaust Valves	44
5.5	Total Gas, Fresh Air and Residual Gas Mass	46
5.6	Composition Fraction	48
5.7	Measured and Estimated Temperatures	49
5.8	Computational Expenses for each Test	53
5.9	Temperature at Point A, 70° BTDC	57
6.1	Sensitivity of Air Mass to T_{IVC} and T_{EVC}	61
6.2	Sensitivity of Air Mass to Cylinder Wall Temperature	62
6.3	Sensitivity of Air Mass to Intake and Exhaust Valve Lash	63
6.4	Sensitivity of Air Mass to Pressure Pegging	64
B.1	Test 1- IVO:-354.7; IVC: -162.8; EVO: 144.3; EVC: 350.2	74
B.2	Test 2- IVO:-354.7 ; IVC: -162.8; EVO: 144.3; EVC: 350.2	75
B.3	Test 3- IVO:-354.7; IVC:-162.8; EVO:144.3; EVC:350.2	76
B.4	Test 4- IVO:-354.7; IVC:-162.8; EVO:144.3; EVC:350.2	77
B.5	Test 5- IVO:-354.7; IVC:-162.8; EVO:144.3; EVC:350.2	78
B.6	Test 6- IVO:-339.7; IVC:-147.8; EVO:129.3; EVC:335.2	79
B.7	Test 7- IVO:-339.7; IVC:-147.8; EVO:129.3; EVC:335.2	80
B.8	Test 8- IVO:-339.7; IVC:-147.8; EVO:129.3; EVC:335.2	81
B.9	Test 9- IVO:-324.7; IVC:-132.8; EVO:114.3; EVC:320.2	82
B.10	Test 10- IVO:-324.7; IVC:-132.8; EVO:114.3; EVC:320.2	83
B.11	Test 11- IVO:-324.7; IVC:-132.8; EVO:114.3; EVC:320.2	84
B.12	Test 12- IVO:-309.7; IVC:-117.8; EVO:99.3; EVC:305.2	85

Notation

ABBREVIATIONS

Abbreviation	Description
IC	Internal Combustion
EC	External Combustion
SI	Spark Ignited
CI	Compression Ignited
VVT	Variable Valve Timing
EGR	Exhaust Gas Recirculation
IVO	Intake Valve Opening
IVC	Intake Valve Closing
EVO	Exhaust Valve Opening
EVC	Exhaust Valve Closing
TDC	Top Dead Center
BTDC	Before Top Dead Center
ATDC	After Top Dead Center
CAD	Crank Angle Degree
IMPR	Intake Manifold Pressure Referencing
PIPR	Polytropic Index Pressure Referencing
OF	Overlap Factor

1

Introduction

This chapter gives a brief background, states the purpose of this master thesis and provides an overview of the main parts covered in this report.

1.1 Background

Nowadays, there is an increasing demand for improving engine performance in order to fulfill customer expectations, meet more restrictive environmental regulations and release less emissions into the atmosphere. To improve the engine performance, its influential parameters should be recognized. The most important of these parameters are summarized below [8]:

- The amount of air sucked into the engine cylinder during the intake stroke.
- The amount of fuel injected into the cylinder and fuel injection pressure.
- The amount of recirculated gases.
- The amount of residual gas remained in the cylinder from the previous cycle.
- Combustion timing including the time of injection and ignition.
- Pressure in the intake and exhaust manifolds, whether throttle and/or turbocharger is used or not.
- Timing of intake valve opening and closing.
- Timing of exhaust valve opening and closing.

Among all the influential factors, the determination of the cylinder charge gas has been given a particular attention and the difficulty is due to the fact that the amount of residual gas and fresh air mass varies by many different parameters such as the pressure in the intake and exhaust manifolds, valve phasing, valve overlap as well as the operating conditions. Thus, accurate estimation of the gas amount and composition yields better engine functionality, performance and fuel economy.

1.2 Goal and Purpose

A classical method for the determination of fresh air mass entering the cylinder is to mount an air flow meter in the intake manifold and record the values by running the engine under different operating conditions. However, the response delay and low level of accuracy in the transient conditions limit the reliability of this type of measurement [2, 10]. Moreover, it adds a cost when this sensor is used in production engines even if the before-mentioned drawbacks are ignored or overcome.

One of the beneficial features of the cylinder pressure sensors is their fast dynamic response compared to air flow meters. Therefore, one approach to eliminate these deficiencies is to construct a pressure-dependent model. The other beneficial merit is that the results can be validated by those obtained experimentally when there is negative valve overlap and the engine is running under steady-state condition. Next, this model can be used/adapted to predict the gas mass composition when there is a positive valve overlapping or the engine runs under transient conditions.

Therefore, this thesis work is aimed to find a suitable thermodynamic method for estimating the in-cylinder trapped gas mass including the fresh air, fuel, residual gas and potentially blow-by as well as their summation either as a part of a lab measuring procedure using the in-cylinder pressure sensors, or as a real-time method for implementation in an engine control unit that are not equipped with the cylinder pressure sensors. The proposed model(s) should estimate the total gas mass and its composition in different operating conditions, with the relative errors lower than $\pm 3\%$.

1.3 Thesis Outline

The work done during this master thesis and the concepts contained in this report are described in the following chapters.

Chapter 2 presents some necessary background information about internal combustion engines and the four-stroke engine cycles. The most commonly used definitions and expressions are also explained.

In **Chapter 3** Various approaches for the mass, heat transfer and temperature estimation are investigated.

Chapter 4 provides a thorough knowledge about the method proposed in this master thesis, its application, assumptions and limitations.

In **Chapter 5** the results are indicated and discussed. Any agreement or disagreement with the literature review and physical response of the engine is also addressed. Besides, some possible sources of error and how they affect the result are described. Computational cost is also taken into account and its importance versus the level of accuracy is also studied in this chapter.

Since the aim is to build a robust model with the lowest level of sensitivity, **Chapter 6** aims to investigate the influence of change of different parameters in the output(s). Also, the least and most sensitive conditions are stated accordingly.

In **Chapter 7**, the most important findings of this thesis work are highlighted.

Finally, **Chapter 8** is dedicated to the potential future work and points out some ideas for further investigations to improve the level of accuracy.

2

Internal Combustion Engines

2.1 Background

Combustion engines are designated to convert chemical energy of the fuel, via thermal energy, into mechanical work. In general, engines can be categorized into Internal Combustion (IC) and External Combustion (EC) engines. IC engines, which are the focus of this study, are those where the combustion of fuel takes place inside the engine cylinder whilst the fuel is combusted outside the engine in EC engine and the released heat is passed to the in-cylinder gases.

IC engines can be classified based on the fuel type, number of strokes per each working cycle or combustion strategy. The fuel can typically be gasoline, natural gas, bio-gas, diesel, hydrogen and so forth. The number of strokes in one complete working cycle is related to the piston movement and can typically be either two or four. In two-stroke engines, the power is generated with two strokes of the piston during one crank angle revolution while in the four-stroke engines, the power cycle completes after four strokes of the piston. Note that the focus is on the engines with four-stroke cycles in the rest of this report. Another classification is based on the combustion process, by which the IC engines can be categorized into Spark Ignited (SI) and Compression Ignited (CI) engines.

Vehicles with SI engines were traditionally equipped with a carburetor to measure the sufficient amount of fuel needed to mix with the air before entering the engine. Nowadays, the fuel flow is controlled by fuel injection control systems [8]. The recent technologies in these engines are such that the fuel is injected either in the intake system or during the intake or early in the compression stroke so that the fuel is given enough time to be mixed with the air and create a homogeneous mixture before the spark ignites the mixture [8].

In CI engines, the combustion is initiated by the start of injection and is characterized by the three main phases, ignition delay, premixed combustion and

mixing controlled combustion [8]. The liquid fuel injected into the combustion chamber must be heated up to a vapor so that it can auto-ignite [8]. The time from the start of injection to start of combustion is called the ignition delay [8]. The fuel will be combusted when the temperature is equal or above the auto-ignition temperature of the fuel. This phase is called the premixed combustion phase. Finally, the fuel mixes with the air and burns during the third combustion phase called mixing controlled phase [8].

2.2 The Four Stroke Engine Cycle

The four processes in the engine cylinder in sequential order are as follows,

Intake: Inlet valve opens around TDC and closes around BDC. While the piston is moving downwards, the air/air-and-fuel mixture travels from intake manifold into the cylinder. The amount of air sucked into the cylinder is a function of valve profile, fresh-charge velocity and pressure difference between intake manifold and cylinder; however, this pressure difference is not large, especially at BDC [8].

Compression: After inlet valve closes, the air/air-and-fuel mixture is compressed meanwhile the piston is traveling upwards from BDC to TDC; the temperature and pressure of the in-cylinder gases increase steeply and the fuel is injected into the cylinder. The mixture is ignited either by a spark or by the in-cylinder hot gases, depending on the type of IC engine, and combustion is initiated [8].

Expansion: The flame propagates gradually and the heat is released from the mixture such that the work produced moves the piston from TDC to BDC. The exhaust valve opens to guide the burned gases towards the exhaust port and the cylinder gets ready for the fresh air to enter the cylinder.

Exhaust: The gas is pushed out from cylinder into the exhaust port while the piston is traveling from BDC to TDC.

The aforementioned process is known as the traditional working cycle in reciprocating engines. Nowadays, some improvements are made in the valve timings and start of combustion to generate more work during expansion and create less emission out of combustion chamber. For instance, the intake and exhaust processes are modified such that the scavenging and ram effect concepts are utilized and the engine performance is subsequently improved. Note that there are also some other differences between classical and newly-developed IC engines that is not mentioned here.

Figure 2.1 demonstrates the four-stroke operating cycle used in both SI and CI engines.

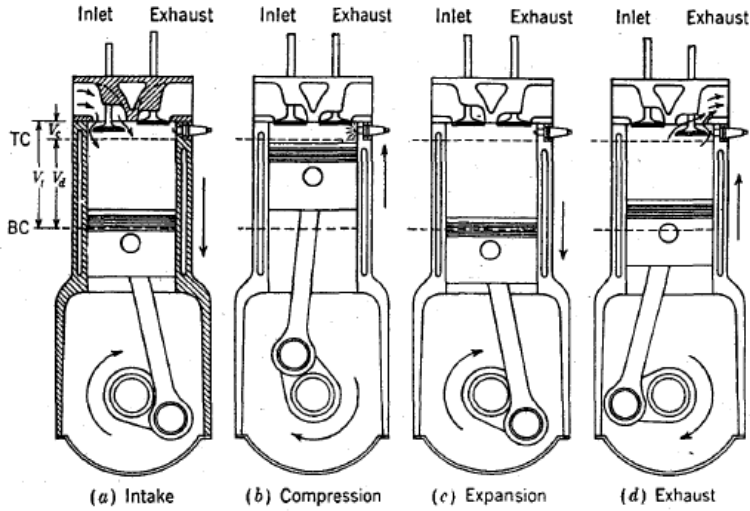


Figure 2.1: The Four-Stroke Operating Cycle [12]

2.3 Definitions

In this section, the expressions and definitions used in this report are explained, and if applicable, the corresponding mathematical equations are presented.

2.3.1 Valve Timing

Valve timing defines the crank angle at which the intake or exhaust valve opens and closes. When the Exhaust Valve Opening (EVO) happens early, less work is generated during the expansion stroke since the cylinder pressure is reduced. On the other hand, if the exhaust valve opens late, the gas pressure becomes higher and thus, higher pumping work is needed [8]. If the Exhaust Valve Closing (EVC) happens early, more residual gases are trapped in the cylinder and these gases are re-compressed when the piston is close to the Top Dead Center (TDC). Conversely, if EVC is delayed, the engine cylinder is better emptied and more ready to be filled with fresh air. Furthermore, when Intake Valve Opening (IVO) happens early, the residual gases travel into the intake manifold while the later intake valve is opened, the entry of air or air-and-fuel mixture from the intake manifold is restricted. The timing of Intake Valve Closing (IVC) controls the amount of total mass trapped in the cylinder. Therefore, it can be generally stated that intake and exhaust valve timings influence the generated expansion work, residual gas mass, blow-down and pumping losses [8].

Considering the aforementioned events, when modeling the residual gas mass, a special attention must be given into the part from EVO to IVC as it can strongly influence the amount of residual gas mass trapped in the cylinder. Figure 2.2

displays an example of intake and exhaust valve lift profiles, valve timing and spontaneous engine cylinder.

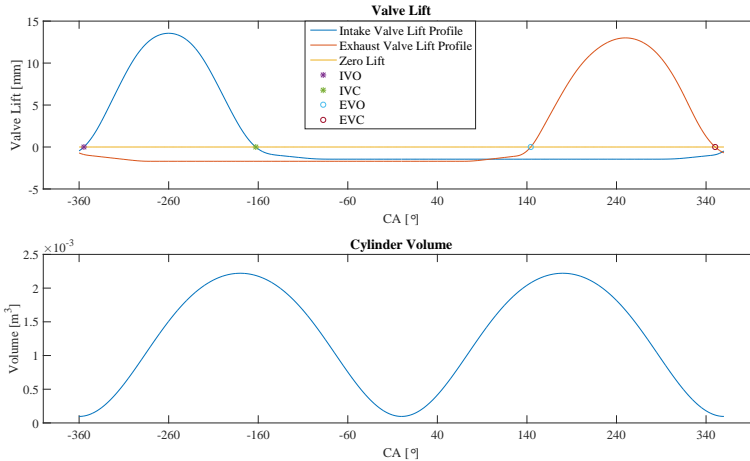


Figure 2.2: Valve Lifts and Cylinder Volume

In general, valve-train, valve profiles and timings, controls gas exchange process and affects combustion and engine torque [8]. In a fixed cam engine, the valve profiles and timings are typically chosen by compromising between the engine performance at high and low loads as well as high and low engine speeds; nevertheless, this trade-off is removed in Variable Valve Timing (VVT) engines [8]. In the cycle shown in figure 2.2, the intake valve opens just after TDC and closes after 191.9°, around 20° after BDC. Afterwards, exhaust valve opens at 140° after TDC and closes after 205.9°.

Valve Overlap

Valve overlap is the time over which the intake and exhaust valves are both open; therefore, it can be either positive or negative. The negative valve overlap means that the exhaust valve is closed prior to the opening of the intake valve. As a result, no scavenging occurs. Positive valve overlap, on the other hand, is when the exhaust valve closing takes place after the opening of the intake valve; this implies that scavenging or blow-by is possible and its magnitude is dependent on the engine speed, the degree of valve overlap and the pressure difference between the intake and exhaust manifolds.

When there is a positive valve overlap, the amount of residual gas mass is controlled by the valve timing, in-cylinder pressure, intake and exhaust manifold pressures and many other parameters. For instance, if the intake pressure is higher than the exhaust pressure, scavenging occurs which means the fresh air travels from the intake to the exhaust manifold taking a part or all of the residual gases with it out of the cylinder.

In contrast, when the pressure in the intake manifold is less than that in the exhaust manifold, back-flow takes place and a part of exhaust gas comes back into the cylinder and then into the intake manifold due to the reverse pressure difference. In this case, this back-flow returns back into the cylinder during the next intake stroke, causing a larger residual gas mass since more gas mass remains/returns back into the cylinder from the previous cycle.

2.3.2 Volumetric Efficiency

Volumetric efficiency is a measure of the effectiveness of the engine during the intake stroke [12]. In simple words, it is the ratio between the volume of the fresh air in the cylinder and the displaced volume of the engine [8]. Note that the volumetric efficiency can be used for the four stroke engines, both SI and CI engines, and it usually is at maximum around 80 to 90 percent for the naturally aspirated engines; however, it is typically higher for diesel engines than for the SI engines [12]. If the intake runners are well-tuned, the volumetric efficiency can exceed unity [8].

$$\eta_v = \frac{V_a}{V_d} \quad (2.1)$$

where V_a and V_d denote for the air volume and displaced volume, respectively.

2.3.3 Residual Gas, EGR, Blow-By and Back-Flow

As mentioned previously, residual gas is a component of the total in-cylinder gas that remains in the cylinder from the previous cycle and can be determined by studying the intake and exhaust processes [12]. In another words, not all the gas entering the cylinder during the intake stroke leaves the cylinder during the exhaust stroke due to the fact that at the end of exhaust process, e.g. the clearance volume is still occupied by the burned gases and the difference between the amount of gas in the intake and exhaust is the residual gas [8]. The residual gas fraction affects the volumetric efficiency, i.e it occupies a portion of cylinder volume that could have been filled with the fresh air and fuel instead, and engine performance because its magnitude and temperature influences the composition and the thermodynamic properties of the gas trapped in the cylinder [8, 12]. Factors such as valve timing, compression ratio, engine speed, intake and exhaust pressures can influence the residual gas fraction [12]. Due to higher compression ratio in diesel engines and the larger difference between the exhaust and intake pressures, residual gas fraction is lower in diesel engines compared to that in gasoline engines [12].

The total mass in the combustion stroke is the sum of the fresh air, fuel and the residual gas mass as stated below,

$$m_{tot} = m_{air} + m_f + m_{res} \quad (2.2)$$

Exhaust Gas Re-circulation (EGR) is defined as the external re-circulation of the exhaust gases into the intake manifold. Note that the residual gases are sometimes considered as the internal EGR [8].

Moreover, in the situations where the pressure in the intake manifold is higher than that in the exhaust manifold, some of the fresh air that is sucked into the engine leaves the cylinder through the exhaust manifold [12]. This phenomenon is known as blow-by or scavenging and can only occur when there is an overlap between the opening of the intake and the exhaust valves.

In contrast, back-flow occurs when the pressure at the exhaust manifold is higher than that in the intake manifold, so some of the gas travels from the exhaust to the intake and enters the cylinder during the next intake stroke. Back-flow from the exhaust manifold has a contribution to the residual gas [8].

3

Research Study

The first step is to conduct an investigation on the most typical solutions to the given problem. The aim is to get up to date with different approaches to the main target, understanding the pros, cons and potential challenges of each approach and familiarizing with the topic. Thus, this chapter reviews a wide range of methods investigated recently.

3.1 Gas Mass Estimation

The methods for charge determination are mainly based on the results obtained from the specific sensors located in the cylinder or in the vicinity of the intake or exhaust manifolds [6].

By measuring the cylinder pressure profile, solving the ideal gas law for the mass in the cylinder requires information about a temperature during the compression or expansion; however, measurements of the in-cylinder temperature are difficult and may not be accurate enough [24]. Accurate temperature measurement is crucial since any deviation from the actual temperature causes an error in the trapped gas mass calculation. Hence, different methods are investigated to estimate the total gas mass trapped in the cylinder and its composition.

In the following sections, the main principles behind the most important of these methods are explained.

3.1.1 Standard Volumetric Efficiency Method

In this method, hot wire anemometer is used for calculating the mass flow of air entering the engine. Additionally, the intake manifold pressure and temperature can be obtained, for example, by the use of piezo-resistive and thermo-resistive sensors, respectively [6, 9].

$$\dot{m}_{tot} = \eta_v \frac{p_{int}}{RT_{int}n_r} N_e V_d \quad (3.1)$$

In this equation, η_v , p_{int} , T_{int} , R , N_e , V_d are the volumetric efficiency, intake manifold pressure, intake manifold temperature, ideal gas constant, engine speed and displaced volume, respectively. Beside, n_r is the number of revolutions per stroke which is 2 for four-stroke engines.

In the absence of EGR, air is the only component entering the cylinder. Thus, once the intake gas condition is known, the volumetric efficiency can be computed from the equation above, which can be used in the on-board conditions to calculate the total trapped mass. When EGR is used, however, the fresh air and recirculated exhaust gas both enter the engine through the intake manifold. In this condition, the following equation can be used to predict how much EGR enters the engine,

$$\dot{m}_{EGR} = \dot{m}_{tot} - \dot{m}_{air} = \eta_v \frac{p_{int}}{RT_{int}} N_e V_d i - \dot{m}_{air} \quad (3.2)$$

The remarkable merit of this method is that it is easy to implement; however, since it relies on the measurement obtained from the mass air flow meter, it may lack accuracy in transient conditions. η_v also depends on the operating conditions, with the strongest dependence on the engine speed and intake pressure, but also on exhaust pressure. η_v , therefore, needs to be mapped or modeled in some way, and with the introduction of VVT, the valve settings influences η_v as well.

3.1.2 Δp Method

This method is based on the engine's behavior in the compression stroke and aims at relating the trapped mass to the evolution of pressure between two arbitrary points, referred to as a and b . In this approach, the ideal gas law together with the isentropic relations are used to calculate the total trapped mass in the cylinder [6, 9].

$$\Delta p = p_b - p_a = p_a \left(\left(\frac{V_a}{V_b} \right)^k - 1 \right) \quad (3.3)$$

As shown in the equation, the compression process between points a and b is assumed to be isentropic and k is c_p/c_v . Using the state equation at the point a yields the following equation,

$$\Delta p = \frac{m_{IVC} R T_a}{V_a} \left(\left(\frac{V_a}{V_b} \right)^k - 1 \right) \quad (3.4)$$

where in this equation, the IVC stands for the condition when the intake valve is closed. Finally, by the rearrangement of the equation (3.4), the total trapped gas mass can be obtained as,

$$m_{IVC} = \frac{\Delta p V_a}{R T_a} \left(\left(\frac{V_a}{V_b} \right)^k - 1 \right)^{-1} \quad (3.5)$$

where b can be any point after IVC and before start of fuel injection and k is the polytropic coefficient during compression stroke. Note that the composition of gases in the cylinder and the ideal gas constant change during the compression stroke, especially when combustion initiates; thus, selection of point b is of high importance; if it locates close to IVC, the selected interval for the Δp becomes narrow and compression characteristics are not predicted correctly; also, it also should not be far from point a , or IVC otherwise this point may interfere with the fuel injection time [10].

As can be seen in equation (3.5), the volume at the two predetermined crank angles and the constants R and k are known while the temperature at the initial point is either known or estimated. R can be assumed constant over a wide range of temperature and pressure. In addition, when EGR is used, the gas composition also have an impact on R . Polytropic coefficient k is strongly dependent on the operating conditions, but it can be treated as constant in this approach.

Moreover, the temperature at point a must be calculated accurately because it is affected significantly by the operating conditions and other influential factors i.e. the atmospheric conditions temperature, boost pressure, compressor efficiency, exhaust temperature, EGR rate, EGR cooler efficiency, residual gas fraction and its temperature, heat transfer from the cylinder wall to the intake runners and the trapped mass until point a is reached.

Due to the aforementioned reasons and noting that the temperature T_a cannot be measured experimentally in the test cells, models are used to express the T_a based on the other known engine variables [2, 6, 9]. Hence, the better the estimation of the temperature at point a , the more accurate the determination of the mass inside the cylinder. There are different approaches for determining the reference temperature, T_a , some of which are discussed in the following paragraphs.

As stated in equations (3.1) and (3.5), both the volumetric efficiency and the temperature at point a are strongly dependent on operating conditions. According to [6], linear and quadratic correlations can be used as represented below,

$$\frac{m_{tot} T_{int}}{p_{int}} = [a_1, a_2, a_3, a_4, a_5, a_6, a_7] \times [1, N_e, p_{int}, \frac{p_{exh}}{p_{int}}, T_w, T_{int}, m_f]^T \quad (3.6)$$

$$\frac{m_{tot}}{\Delta p} = [b_1, b_2, b_3, b_4, b_5, b_6, b_7] \times [1, N_e, p_{int}, \frac{p_{exh}}{p_{int}}, T_w, T_{int}, m_f]^T \quad (3.7)$$

To make the correlation less complicated, quadratic dependency is only used for the engine speed and the injected fuel mass as shown below,

$$\frac{m_{tot} T_{int}}{p_{int}} = [c_1, c_2, c_3, c_4, c_5, c_6, c_7, c_8, c_9, c_{10}] \times [1, N_e, p_{int}, \frac{p_{exh}}{p_{int}}, T_w, T_{int}, m_f, N_e^2, N_e m_f, m_f^2]^T \quad (3.8)$$

$$\frac{m_{tot}}{\Delta p} = [d_1, d_2, d_3, d_4, d_5, d_6, d_7, d_8, d_9, d_{10}] \times [1, N_e, p_{int}, \frac{p_{exh}}{p_{int}}, T_w, T_{int}, m_f, N_e^2, N_e m_f, m_f^2]^T \quad (3.9)$$

However, in [2], T_a is computed from the following equation,

$$T_a = c_0 + c_1 N_e^2 + c_2 m_f^2 + c_3 \frac{1}{N_e^3} + c_4 m_f^3 N_e \quad (3.10)$$

Note that the fuel mass can be used as that estimated by the electronic control unit, even though some major deviations can possibly take place [6]. Comparing equation (3.6) (or (3.8)) with equation (3.10), it can be said that the latter approach requires less measured variables. Besides, for defining the T_a from equation (3.6) or (3.8), some of the variables must be measured by the use of sensors; this leads us to conclude that the real time implementation by the latter approach is more feasible [2]. However, since the influence of the wall temperature is not included in equation (3.10), it may give less accurate estimation of the in-cylinder trapped mass in the cold start conditions.

The total mass entering the cylinder can be stated as the sum of the fresh air mass and EGR. The idea in [2] is that EGR is derived from the CO_2 measurement in the intake and exhaust manifolds. In this approach, neither the residual mass nor the back-flow were considered due to their minor influence in the mass flow calculations. It is also worth mentioning that the pressure interval between points a and b affect the accuracy of the results [2].

3.1.3 Correlation Method

This approach, which is proposed by Akinoto and Itoh, is also called the Δp method with a bit more complex computational costs [24]. The equation (3.5) can be rewritten in the following way,

$$m_{IVC} = \frac{V_a V_b^k \Delta p}{RT_a (V_a^k - V_b^k)} \quad (3.11)$$

Since m_{IVC} is the total trapped gas mass in the cylinder, the fuel and the residual gas mass can be subtracted from the total mass to obtain the mass of air entering the cylinder, m_{air} , as indicated in the following equation,

$$m_{air} = \frac{V_a V_b^k \Delta p}{RT_a (V_a^k - V_b^k)} - m_f - m_{res} \quad (3.12)$$

To express this equation in a simple manner, all the terms multiplied by Δp are compacted and shown as α and the term β stands for the mass of fuel and residuals. By doing so, the following equation can be obtained,

$$m_{air} = \alpha \Delta p - \beta \quad (3.13)$$

where,

$$\alpha = \frac{V_a V_b^k}{RT_a (V_a^k - V_b^k)} \quad (3.14)$$

and

$$\beta = m_f + m_{res} \quad (3.15)$$

Equation (3.13) is a straight line with α as the slope and β being the y-intercept of the straight line when plotting the mass of air as a function of the in-cylinder pressure difference calculated between the two points in the compression stroke. Both m_{air} and Δp and their correlation can be obtained experimentally. After calculating α and β , the fresh charge can be calculated from equation (3.13).

3.1.4 Fitting Pressure Trace During Compression

The methodology resembles the Δp method where the compression stroke is the main focus. In this approach, the cylinder pressure is estimated by using the intake and exhaust manifold pressure. Next, the estimated cylinder pressure is compared to the measured one with the aim of lowering/minimizing the error between them; afterwards, the total mass in the cylinder can be computed the temperature in compression stroke is known; this method also needs the cylinder wall temperature to quantify the heat transfer during the intake stroke [10].

A domain in the compression stroke is selected a few degrees after the intake valve is closed, and due to the polytropic relation governing the flow behavior in the compression, equation (3.3) holds between any two arbitrary points in this domain. Next, the in-cylinder temperature is calculated from the following equation by an estimated cylinder mass,

$$\hat{T}_{cyl}(i, \alpha) = \frac{p_{cyl}(\alpha) V_{cyl}(\alpha)}{\hat{m}_{tot}(i) R} \quad (3.16)$$

where i and α denote the iteration number and crank angle, respectively. Note that the computation is performed at several crank angles and the estimated values are distinguished by the use of hat notation on the top; thus, the estimated cylinder pressure can be calculated from the temperatures obtained in the previous step according to the following equation,

$$\hat{p}_{cyl}(i, \alpha) = p_{cyl}(\alpha) \left(\frac{\hat{T}_{cyl}(i, \alpha)}{\hat{T}_{ref}(i)} \right)^{\frac{k(\alpha)}{k(\alpha)-1}} \quad (3.17)$$

Finally, the error between the measured and the estimated pressures is minimized as the follows,

$$\varepsilon(i) = \sum_{\alpha=1}^{n_{\alpha}} \frac{\hat{p}_{cyl}(i, \alpha) - p_{cyl}(\alpha)}{n_{\alpha}} \quad (3.18)$$

By using an iterative approach, the in-cylinder mass is adapted in such a way that the estimated pressure converges the measured cylinder pressure. Beside this iterative method, the residual gas mass is determined using another model that compares the CO_2 before combustion with that in the exhaust gasses [10]. Finally, the fresh air mass can be computed from the following equation,

$$\hat{m}_{air}(i) = \hat{m}_{tot}(i) - \hat{m}_{res}(i) \quad (3.19)$$

3.1.5 Frequency Analysis of the Pressure Trace

The frequency of the pressure oscillation in the cylinder is studied in this method. This frequency can be influenced not only by the speed of sound, but with the geometry of the engine as well, as stated in the equation below,

$$f_{cyl} = \frac{cB}{\pi D} \quad (3.20)$$

where c represents the speed of sound, D is the cylinder diameter which is also known as the cylinder bore and B is the Bessel coefficient for the first radial mode. The speed of sound is temperature dependent and therefore, varies with the crank angle and the Bessel coefficient depends on the engine geometry [11]. Since the engines geometry is given and fixed in this work, Bessel coefficient as well as the speed of sound are only dependent on the crank angle.

The speed of sound can be obtained from the following equation,

$$c = \sqrt{\gamma RT} = \sqrt{\frac{\gamma p V}{m_{tot}}} \quad (3.21)$$

Insertion of equation (3.21) into (3.20) and rearrangement gives,

$$m_{tot} = \left(\frac{B(\alpha) \sqrt{\gamma p(\alpha) V(\alpha)}}{\pi D f_{cyl}(\alpha)} \right)^2 \quad (3.22)$$

After determination of the total gas mass trapped in the cylinder, the temperature when the exhaust valve opens can be calculated by using the ideal gas law as below,

$$T_{EVO} = \frac{P_{EVO} V_{EVO}}{m_{tot} R_{EVO}} \quad (3.23)$$

The exhaust is modeled as an isentropic process as shown below,

$$T_{EVC} = T_{EVO} \left(\frac{P_{EVC}}{P_{EVO}} \right)^{\frac{k-1}{k}} \quad (3.24)$$

Finally, to obtain the residual gas mass from the ideal gas law at EVC, the following equation yields,

$$m_{res} = \frac{P_{EVC} V_{EVC}}{R_{EVC} T_{EVO} \left(\frac{p_{EVC}}{p_{EVO}} \right)^{\frac{k-1}{k}}} \quad (3.25)$$

where m_{res} stands for the residual gas mass.

3.1.6 Other Methods

Here, a non-pressure based method declares that the amount of fresh charge in the cylinder can be computed if the precise data about air to fuel ratio, A/F , and the burned fuel mass are available [24]; so, the mass of air can be obtained from the following equation,

$$m_a = m_f \frac{A}{F} \quad (3.26)$$

where A/F ratio at the steady state condition can be determined by the analysis of the exhaust gas; additionally, the mass flow rate of fuel can provide information about the injected fuel in the cylinder [24]. These data give us the mass of air in the cylinder through the equation (3.26); however, it lacks accuracy in the transient conditions [24].

It is important to note that only the trapped air mass can be determined through the application of this method. Therefore, it must be used with another method to provide information about the composition of the trapped gas mass.

3.2 Heat Transfer

Generally speaking, the heat generated by the combustion can be transferred to the working gas or the chamber walls; therefore, heat transfer is needed for the energy balance in the combustion chamber.

Since the in-cylinder gas pressure and temperature varies significantly throughout each engine cycle, the detailed analysis of the heat transfer is complex and computationally expensive. Nevertheless, previous investigations prove that heat loss across the chamber wall to the surrounding is an important part of the total heat released from the fuel, and can be a small negative value during the intake process to a considerably large and positive value during the expansion [12, 18].

Convection and radiation modes of heat transfer takes place in the cylinder. In SI engines, radiation accounts for around 3 to 4 percent of the total heat transfer during combustion; this value increases up to 10 percent for the diesel engines due to soot formation during combustion [21]. However, since the heat transfer during the gas exchange process is interesting in this work, radiation is negligible and only convection is discussed in the following section.

Equation for the convection heat transfer mode is as below,

$$\dot{Q}_{wall} = h_g A (T_g - T_w) \quad (3.27)$$

where h_g is the convection heat transfer coefficient, A is the cylinder surface area, T_g is the gas temperature and T_w is the cylinder wall temperature. It can be easily seen that the main parameter to define is the heat transfer coefficient, h_g .

One of the important points at this stage is to distinguish the time-averaged heat flux, instantaneous spatially-averaged heat flux and instantaneous local heat fluxes to the cylinder wall. The critical gas properties for the aforementioned correlations are as follows:

- Gas velocity to calculate the Reynolds number
- The gas temperature at which the gas properties are evaluated
- The gas temperature used in the convection equation, (3.27)

3.2.1 Correlation for Time-Averaged Heat Flux

The overall heat-transfer correlation is obtained by the work of Taylor and Toong studying 19 different engines. They relate the Reynolds number to convective heat flux and the results are shown in figure 3.1 where the Nusselt number is plotted against the Reynolds number.

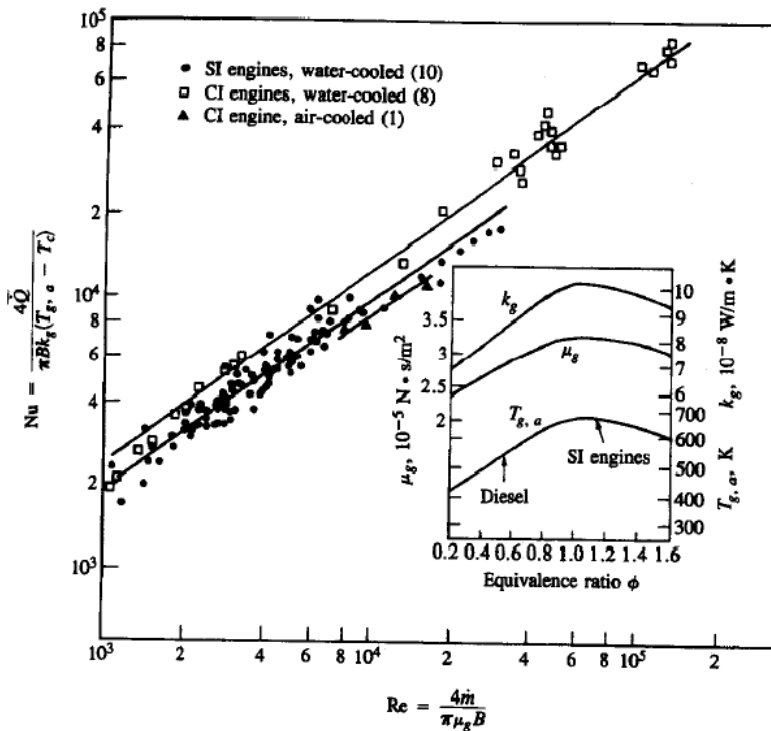


Figure 3.1: Overall engine heat-transfer correlation for different types of IC engines [12]

Note that in this figure, \dot{m} , k_g , μ_g and T_g are mass flow rate, thermal conductivity of the gas, gas velocity and the mean effective gas temperature, respectively.

Modified Eichelberg Heat Transfer Model

The heat transfer is modeled using the Eichelberg model with some modification to obtain an increased temperature. This model is as below,

$$\Delta T_{ht} = c \frac{V_{mp}^{\frac{1}{3}} \sqrt{p_{int} T_{mix}} A (T_w - T_{mix})}{m_{IVC} c_{p,IVC}} \quad (3.28)$$

where V_{mp} is the mean piston speed, p_{int} is the intake manifold pressure and c is the model constant. Finally, the temperature in the intake manifold can be computed from the following equation,

$$T_{ref} = T_{IVC} + \Delta T_{ht} \quad (3.29)$$

where T_{ref} , the reference temperature, is the temperature at the initial point of Δp method.

3.2.2 Correlation for Instantaneous Spatial-Averaged Heat Flux

The convection itself can be either natural or forced convection. Since the movement of the working fluid in the chamber is governed by an external factor, it is more reasonable to assume the heat transfer undergoes the forced convection. Researches have been conducted over the years to determine this heat transfer coefficient precisely. Most of the work is aimed at obtaining the spatially-averaged value for the cylinder, which is the reason they are commonly referred as the global heat transfer models [18].

Making use of dimensional analysis and some experimental observations, the general formulation for the forced convection instantaneous heat transfer coefficient can be written as,

$$Nu = a Re^m Pr^n \quad (3.30)$$

where Nu , Re and Pr are dimensionless Nusselt, Reynolds and Prandtl numbers. The value for the exponent m has been proposed by different authors, for instance, m is 0.5 for Elser and Oguri, 0.7 for Annand and Sitkei, 0.75 for Taylor and Toong, 0.8 for Woschni and Hohenberg and so on. A detailed examination of Woschni correlation is presented in the next section since it is going to be used in this study.

Woschni Correlation

The Woschni model of heat transfer coefficient is as below [25],

$$h_g = C_0 B^{-0.2} p^{0.8} \left(C_1 V_{mp} + C_2 \frac{V_d T_1}{p_1 V_1} (p - p_{mot}) \right)^{0.8} T^{-0.53} \quad (3.31)$$

where p is the instantaneous pressure in bar, V_{mp} is mean piston speed, B is cylinder bore and C_0 is a value from 110 to 130. The values for C_1 and C_2 are given in the following table,

Table 3.1: C_1 and C_2 Coefficients for Woschni Correlation

Phase	C_1 [-]	C_2 [m/s.K]
Intake-Exhaust	6.18	0
Compression	2.28	0
Combustion-Expansion	2.28	3.24×10^{-3}

As can be seen in equation (3.31), Woschni has two independent terms for the gas velocity. The first term is the un-fired gas velocity and is proportional to the mean piston speed. The second term is the crank-angle, or time, dependent gas velocity induced by the combustion and is proportional to the pressure difference between motoring and firing conditions [25].

One of the difficulties in the use of Woschni correlation is its need to determine the motoring pressure; however, since only heat transfer during the exhaust and intake processes are considered in this study, the second term in the gas velocity estimation vanishes and the expression becomes less complex. Besides, compared to the other heat transfer correlations, the Woschni model is less computationally expensive [18].

3.2.3 Correlation for Instantaneous Local Heat Flux

This approach does not rely on the average gas temperature, but needs to determine the local gas temperature at any time in the cylinder. Another alternative is to divide the combustion chamber into different zones, each having their own representative temperature and heat transfer coefficient. This approach is called zonal modeling, and is typically used for studying the combustion stroke where the gas can have either burned or un-burned content [12].

3.3 Estimation of Cylinder Wall Temperature

There is also a need for calculating the temperature at the cylinder wall during the compression stroke since the heat transfer is between the cylinder gas content and the cylinder wall.

3.3.1 First Method

The cylinder wall thermal state can be determined by the classical techniques; mounting sensors at different parts of cylinder wall and recording the temperature anytime needed. However, it is not feasible to do so due to measurement complexity, cost of sensors that can tolerate extreme conditions in the cylinder and the degree of their reliability. Instead, numerical models can be a proper

alternative. In this section, the thermal state of the gas in the cylinder and the method to predict the cylinder wall temperature are studied.

The method is governed by thermodynamic equations and aims to determine the crank angle at which the heat transfer between the gas and the cylinder wall inverts during the compression stroke. In the early part of the compression, the heat transfer is from the cylinder wall to the gas since the gas temperature is lower than temperature at cylinder wall. As the compression proceeds, the heat transfer inverts and the gas temperature becomes higher than the cylinder wall temperature [1, 3]. The adiabatic condition during the compression stroke, therefore, occurs when the net heat flux is zero and the gas temperature approaches the temperature of the cylinder wall [1, 3].

It is important to note that in this methodology, the time delay between the cause, temperature gradient, and the effect, zero heat flux, is not taken into account; however, a more detailed analysis can show that the time at which the thermal flux is negligible is not necessarily the same as that when there is no temperature gradient [1, 3].

Additionally, thermal state in the combustion chamber is complex, time and spatial dependent. Accordingly, the temperature at the cylinder wall is dependent on the distance from TDC, with higher temperature close to the TDC where the combustion initiates [1, 3]. These effects are not considered when calculating the temperature at the cylinder wall and only one effective wall temperature is estimated.

According to the first law of thermodynamic, conservation of energy, the internal energy of the trapped gas mass, dU , can be related to the piston compression work, δw , and the heat transfer between the piston, cylinder wall and the working fluid, δQ [1, 3]. The mathematical form of the aforementioned statement is as below,

$$dU = \delta Q - \delta w \quad (3.32)$$

This equation, together with the ideal gas law and non-adiabatic polytropic process gives the following equation,

$$\delta Q = -\frac{k - \gamma}{\gamma - 1} p dV \quad (3.33)$$

During the compression stroke, cylinder volume is decreasing while the pressure is increasing; so, the product of $p dV$ is always negative. Having γ larger than one, $\gamma \approx 1.4$, the thermal energy is transferred from the cylinder wall to the in-cylinder gas when $k > \gamma$ and vice versa [1, 3]. In another words, since the cylinder wall temperature is higher than the in-cylinder gas temperature at the early phase of the compression stroke, k will be higher than γ and when the cylinder wall temperature is lower than the in-cylinder gas temperature, k will be lower than γ . Consequently, there exists a crank angle at which $k = \gamma$ corresponding to the zero heat flux between cylinder wall and gas; thus, the average cylinder wall temperature is equal to the gas temperature [1, 3].

Investigating the non-adiabatic polytropic compression process at each crank angle, gas pressure evolves in the following way,

$$p(\theta - \Delta\theta) V(\theta - \Delta\theta)^{k(\theta)} = p(\theta + \Delta\theta) V(\theta + \Delta\theta)^{k(\theta)} \quad (3.34)$$

Rearrangement of this equation leads the estimation of polytropic index as below,

$$k(\theta) = \frac{\log\left(\frac{p(\theta+\Delta\theta)}{p(\theta-\Delta\theta)}\right)}{\log\left(\frac{V(\theta-\Delta\theta)}{V(\theta+\Delta\theta)}\right)} \quad (3.35)$$

This equation can be used at any crank angle between intake valve closing and start of injection. Additionally, γ can be obtained in the following way,

$$\gamma = \frac{c_p(\theta)}{c_p(\theta) - R} \quad (3.36)$$

Figure 3.2 illustrates polytropic index, denoted by m , and specific heat ratio, denoted by k , calculated from (3.35) and (3.36), respectively.

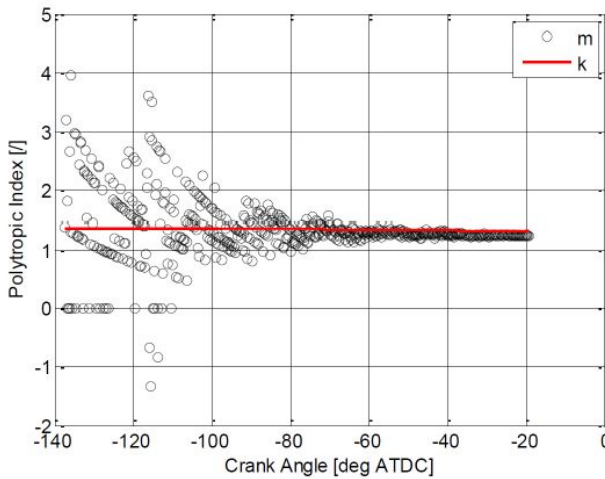


Figure 3.2: Polytypic index and Specific Heat Ratio vs. Crank Angle [3]

When using the experimental data, the polytropic index, k , is fluctuating considerably due to the noisy pressure signal. This fluctuations are much larger at the first stage of the compression stroke. Also note that the polytropic index approaches γ after a while.

It is clear that pressure is increasing during the compression stroke. However, looking at the pressure trace at this stage, some negative pressure gradients can be noticed which is due to the sensor sensitivity. The finding here is that to get a clear trend for the polytropic index and get a well-defined intersection between k and γ , a suitable processing of the experimental pressure signals is required.

To do so, a curve is fitted to the pressure signals during the compression stroke and the pressure increase is obtained subsequently. Therefore, to get the polytropic index, k , the following equation can be used alternatively,

$$k(\theta) = \frac{\log\left(1 + \frac{\Delta p(\theta)}{p(\theta - \Delta\theta)}\right)}{\log\left(\frac{V(\theta - \Delta\theta)}{V(\theta + \Delta\theta)}\right)} \quad (3.37)$$

In this equation, $\Delta p(\theta)$ can be obtained by processing the experimental pressure data through the following equation,

$$\Delta p(\theta) = ab^\theta + c \quad (3.38)$$

where a , b and c can be determined by a non-linear least square fitting curve technique [3].

Finally, plotting polytropic, k , and adiabatic, γ , indexes versus the crank angle, the intersection between the two curves gives the crank angle at which the heat transfer between the cylinder wall and the gas is inverted. Figure 3.3 displays the polytropic index and specific heat ratio obtained by equation (3.37) and 3.36, respectively. Looking at the curves, it can be stated that there might be more than one intersection between the curves; in such a situation, the first intersection is considered as the effective angle at which the heat transfer inversion takes place [3].

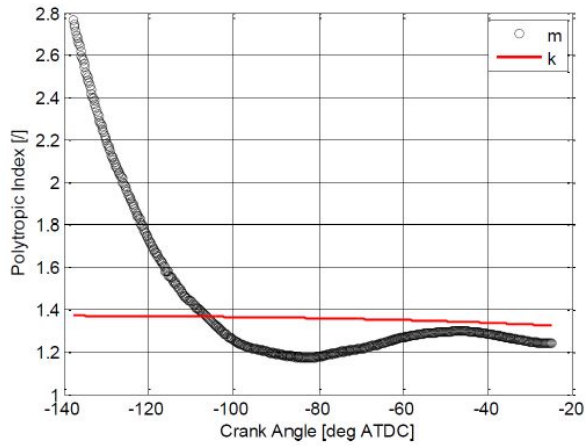


Figure 3.3: Estimated polytropic index and Specific Heat Ratio vs. Crank Angle [3]

3.3.2 Second Method

This method uses an equation for the cylinder wall estimation with its dependency on the engine speed and torque.

$$T_w = c_0 + c_1 Ne + c_2 Tq + c_3 NeTq + c_4 Ne^2 + c_5 Tq^2 + \dots + c_r Tq^s + c_t Tq^u \quad (3.39)$$

where Tq is the engine torque and $c_0, c_1, c_2, \dots, c_t$ are the model constants which can be obtained by a least square curve fitting function to the experimental data.

3.4 Summary

The main focus in this chapter was to introduce some well-known approaches for the estimation of cylinder gas content, cylinder wall temperature and distinguishing between three models for convective heat transfer coefficient.

4

Method

This chapter aims to describe the methodology used for estimating the gas mass in the cylinder and its composition. The proposed model is based on the estimation of residual and total in-cylinder gas masses. First, experimental setup, measured data and operating conditions are stated. Next, input data is summarized and the need for parameter initialization is explained. Finally, the assumptions, their limitations and the most essential equations used in the model are presented.

4.1 Experimental Setup

The experiment is conducted in an engine test cell to measure the cylinder pressure and the mass air flow rate in the intake manifold. The in-cylinder pressure is collected for one complete working cycle as a function of crank angle with the maximum resolution of one sample per 0.1 degree. The crank angle varies from -360° to 360° so that one complete working cycle can be studied. The p-V or indicator diagram visualizes the output of this part of experiment. The experiment also involves measuring the mean pressure and temperature in the intake and exhaust manifolds, average engine speed, engine torque, coolant temperature, air-to-fuel ratio and some other data. Later in the next chapter, all the measured data will be stated for each test, if they are used in the model.

Figure 4.1 displays the engine configuration and sensor locations. As can be seen in this figure, the cylinder pressure sensor is only mounted in cylinder 6 while the temperatures and pressures in the intake and exhaust manifold are measured in all cylinders. Note that turbocharger and turbine are shown for completion and their specifications are not used in this master thesis.

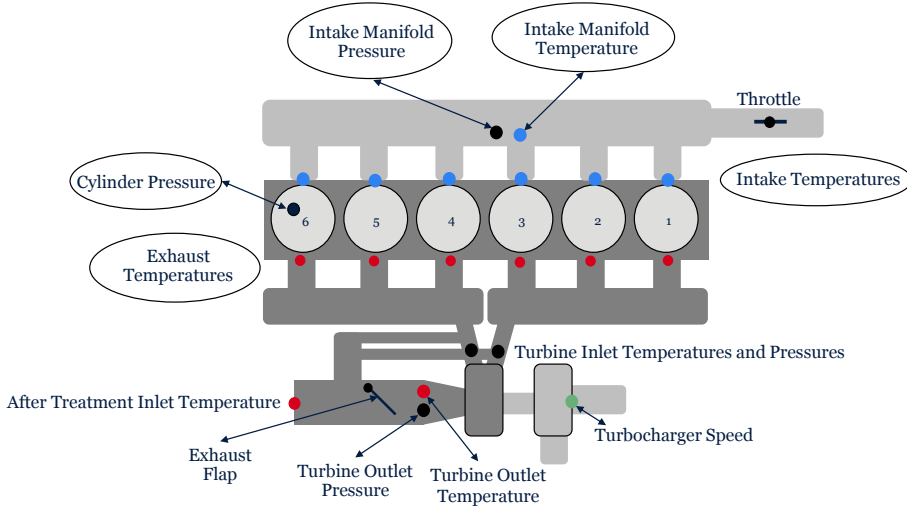


Figure 4.1: Experimental Setup

4.2 Input Data

The engine investigated is a 12.7 liter inline six-cylinder experimental Diesel engine equipped with four valves per cylinder. The engine specifications and the length of connecting rod is stated in the following table.

Table 4.1: Engine Geometry for Diesel Engine

Parameter	Symbol	Value	Unit
Cylinder Bore	B	0.13	m
Piston Stroke	L	0.16	m
Compression Ratio	r_c	23	-
Displaced Volume	V_d	0.0021	m^3
Connecting Rod Length	l	0.2550	m

The instantaneous volume of the cylinder at crank position θ is obtained from the following equation,

$$V_\theta = V_c + \frac{\pi B^2}{4} \left(l + a - (a \cos \theta + \sqrt{l^2 - a^2 \sin^2 \theta}) \right) \quad (4.1)$$

where V_c is the clearance, or minimum, volume of the cylinder and a is the crank radius, where $a = L/2$. The clearance volume is calculated as below,

$$V_c = \frac{V_d}{r_c - 1} \quad (4.2)$$

The data set is composed of 12 different operating conditions, each consist of a number of engine cycles. In total, 60 test cycles are studied as summarized in the table below.

Table 4.2: *Limit Values of the Experimental Data Set*

Parameter	Unit	Lower Value	Upper Limit
Engine Speed	rpm	1200	1800
Torque	Nm	162	2464
Intake Valve Phasing	CAD	0	45
Exhaust Valve Phasing	CAD	-45	0

One of the differences among the tests is the cam phasing and timing adjustment of valve events, where the phase angle of camshaft is shifted forwards or backwards relative to the crankshaft; therefore, direction of deviation from the nominal valve events determines whether the valve is opened/closed early or late. The nominal IVO, IVC, EVO and EVC in the studied engine is -354.7° , -162.8° , 144.3° and 350.2° , respectively. Since the cam mechanism is the same for all the tests, the sooner the intake or exhaust valve is opened, the sooner it is closed and vice versa.

An early closing of exhaust valve traps more residual gases in the cylinder. Despite the aforementioned statement, the longer the exhaust valve is open, the better the engine cylinder is emptied and is ready to be filled with the fresh charge during the next intake stroke [13]. An early opening of intake valve reduces pumping losses while the late closing of intake valve pushes the cylinder gas back into the intake manifold [8, 13]. Intake valve events affect the mixing temperature at IVC, cylinder pressure and temperature in the compression stroke, heat transfer between the gas and neighboring surfaces and the flow from the intake port into the cylinder. In overall, the timing of both intake and exhaust valve events is important to determine the engine behavior.

Another difference among some of the aforementioned tests is combustion phasing. Previous investigations have shown that the ignition timing and combustion phasing affect the engine performance, fuel economy, torque output and emissions and is the most efficient when 50% of the fresh charge is burned 8° ATDC while the engine is running under normal operating conditions [5, 19, 20].

4.3 Pre-processing of in-cylinder pressure signals

Prior to conducting any calculation, the absolute cylinder pressure must be determined precisely, otherwise large errors in the polytropic index computation, mass fraction burned and charge temperature estimations can be seen [4, 16]. To avoid these issues, this section addresses methods to correct the measured cylinder pressure.

4.3.1 The Need for Accurate Absolute Pressure Referencing

Piezoelectric sensors are widely used in the engine cylinder pressure measurements due to their accuracy, fast response time, high durability, appropriate size, bandwidth and low sensitivity to the environmental conditions; however, they only measure the pressure change, not the absolute/total pressure [4, 16]. Since the method proposed in this work is based on the total pressure everywhere in the cylinder, some referencing or pegging of the measured cylinder pressure is essential.

4.3.2 Pressure Offset

The determination of pressure offset is also known as pegging the pressure signal or cylinder pressure referencing and can be done in many different ways, the most prominent of which are the so-called Inlet Manifold Pressure Referencing (IMPR) near BDC, Polytropic Index Pressure Referencing (PIPR), exhaust manifold pressure referencing near exhaust TDC, absolute cylinder transducer referencing exposed to the cylinder charge near BDC and so on [4, 15]. Even though none of these methods are suitable for all operating conditions, the first two above-mentioned methods are the most widely used ones [4, 16].

IMPR method is to reference the experimentally-obtained cylinder pressure to the intake manifold pressure before inlet valve closes [15]. To measure the intake manifold pressure, there are several possibilities such as using one single sensor that is mounted in the inlet plenum measuring the intake manifold pressure for all the cylinders or use of multiple sensors, one for each cylinder [4]. The merit of this method is its relative simplicity; in contrast, its drawback is that the method may become insufficient when the ram effect is considerable [4, 15].

Note that the potential errors by use of this referencing method originate from the deficiencies in measuring intake manifold pressure, intake manifold pressure differences between individual cylinders as well as the error(s) in measuring the cylinder pressure throughout the working cycle [4].

One of the important points at this stage is that the pressure referencing must be done at crank angles where the in-cylinder pressure is constant, for instance where both the intake manifold and cylinder pressure are roughly the same or have the approximately constant difference [15]. The pressure referencing is typically carried out at/around BDC where the difference between the intake manifold pressure and the cylinder pressure is the lowest. According to [4], the best interval is -167° to -162° BTDC, but IVC sometimes happens at -163° BTDC in the investigated tests in this study, so the proposed interval is from -170° to -165° BTDC. The pressure trace in this interval is also examined in order to ensure that it remains fairly constant.

4.4 Assumptions

1. It is assumed that the ideal gas law can be used everywhere in the engine thermodynamic cycle. The ideal gas is a hypothetical gaseous substance

whose molecules do not occupy any volume and the inter-molecular forces are zero [23]. It is obvious that this assumption is only valid at low pressures since the spacing between the gas molecules is large enough that they do not collide. The ideal gas law lacks accuracy at high pressures or low temperatures since the interaction between gaseous components becomes significant [23].

2. The cylinder composition remains unchanged during the exhaust process, from EVO to EVC. This assumption is only valid when the engine is running under negative valve overlap conditions, otherwise the fresh air entering the cylinder affects the cylinder gas composition largely. In such situations, this assumption is valid only from EVO until IVC.
3. Cylinder wall temperature is assumed to be constant and uniform for each cycle and varies only by the operating conditions. In another word, it is assumed that the variations in the cylinder wall temperature can be ignored compared to the variations in the gas temperature [7]. However, in reality, the cylinder wall temperature is dependent on the mode of process in the cylinder and is a function of its distance from the TDC, where combustion initiates.
4. The engine runs at stationary conditions such that the transport properties of the cylinder gas at the start of each cycle is the same as those at the end state of that cycle.
5. Quasi-steady heat transfer model is considered both for the fresh air and the residual gases. Under this assumption, the lag between heat flux and the change in the gas temperature can be neglected.
6. All the heat transfer is between the gas and the cylinder wall, both for the residual and the fresh air gas. However, when the cylinder pressure is higher than the pressure when intake valve opens, the residual gas travels into the intake port and the heat is transferred from the residual gas either to the intake port or to the fresh charge. This charge, then, returns back to the cylinder when the pressure difference is reversed.
7. Variations in the gas temperature and velocity across the combustion chamber is neglected, especially when modeling the heat transfer. Therefore, gas properties are instantaneous spatially-averaged parameters.
8. Only convection is taken into account during the gas exchange process and radiation is neglected.
9. Crevice effects are ignored and the blow-by is assumed to be zero.

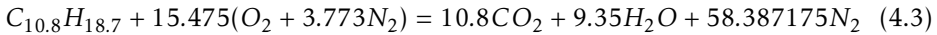
4.5 Chemical Reaction

Burned gas fraction, ideal gas constant and specific heat of the cylinder gases are composition-dependent and the determination of them requires comprehensive

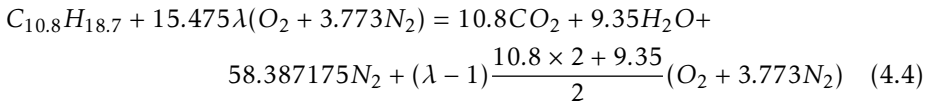
analysis of the cylinder gas content at each stroke. The combustible mixture is composed of the fresh air, fuel and residual gas while the composition of the combustion products can be determined by applying the conservation of mass for each chemical components during the power stroke. For this purpose, the combustion reaction is studied in this section.

It is assumed that the air is composed of 21% oxygen and 79% nitrogen by volume [12]. With the presence of fuel and sufficient amount of air, chemical reactions start when the temperature is high enough. Since the chemical reaction is dependent on the equivalence ratio before combustion starts, two cases are investigated based on the existence/absence of excess air.

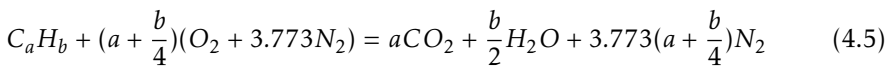
If sufficient air is available, carbon and hydrogen in the fuel are converted into CO_2 and H_2O , respectively. This statement implies that all the fresh air burns during combustion at stoichiometric conditions. For Diesel fuel at stoichiometric condition, the chemical reaction can be written as,



In the presence of excess air, not all the air burns, for which, the chemical reaction is as follows,



where λ is air-to-fuel equivalence ratio. It can be stated that despite equation (4.3), the excess air is presented in the right-hand-side of equation (4.4). The two equations (4.3) and (4.4) can be lumped into one single equation regardless of existence/absence of excess air. In general fashion, for any fuel with any equivalence ratio, the following chemical reaction holds,



Note that the coefficients in all the three aforementioned equations are calculated by the molar balance of components between the reactants and products. Given the fuel and equivalence ratio, the coefficients in equation (4.5) can be determined.

4.6 Ideal Gas Constant, Specific Heat in Constant Pressure/Volume and Burned Gas Fraction

Since the ideal gas constant is composition-dependent, the ideal gas constant of the burned gas differs from that of the fresh air. These two constants are obtained from the following equations.

$$R_{burned} = \frac{aCO_2R_{CO_2} + bH_2OR_{H_2O} + cN_2R_{N_2}}{aCO_2 + bH_2O + cN_2} \quad (4.6)$$

$$R_{air} = \frac{3.773N_2R_{N_2} + R_{O_2}O_2}{3.773N_2 + O_2} \quad (4.7)$$

In these equations, the molecular weight of the compositions are indicated by their chemical formula. It is also worth to mention that for diesel fuel, a , b and c are 10.88, 9.35 and 58.387175, respectively.

The specific heat in constant pressure and volume are both composition- and temperature-dependent. The specific heat of burned gas and air in constant pressure is as follows,

$$c_{p,air}(T) = \frac{O_2c_{p,O_2}(T) + 3.773N_2c_{p,N_2}(T)}{O_2 + 3.773N_2} \quad (4.8)$$

Similarly, the specific heat of the burned gases in constant pressure can be obtained from the following equation,

$$c_{p,burned}(T) = \frac{aCO_2c_{p,CO_2}(T) + bH_2Oc_{p,H_2O}(T) + cN_2c_{p,N_2}(T)}{aCO_2 + bH_2O + cN_2} \quad (4.9)$$

According to [12], the specific heat of the species in equations (4.8) and (4.9) can be obtained from the general equation,

$$c_{p,i}(T) = R_i(a_{i1} + a_{i2}T + a_{i3}T^2 + a_{i4}T^3 + a_{i5}T^4) \quad (4.10)$$

and the constants in this equation are taken from table 4.10 [12]. Finally, the specific heat of different species are as below,

$$c_{p,CO_2} = \begin{cases} R_{CO_2}(0.24 \times 10^1 + 0.873 \times 10^{-2}T - 0.66 \times 10^{-5}T^2 + 0.2 \times 10^{-8}T^3 + 0.632 \times 10^{-15}T^4) & \text{if } 300 < T[K] < 1000, \\ R_{CO_2}(0.44 \times 10^1 + 0.309 \times 10^{-2}T - 0.123 \times 10^{-5}T^2 + 0.227 \times 10^{-9}T^3 - 0.155 \times 10^{-13}T^4) & \text{if } 1000 < T[K] < 5000. \end{cases}$$

$$c_{p,H_2O} = \begin{cases} R_{H_2O}(0.407 \times 10^1 - 0.11 \times 10^{-2}T + 0.415 \times 10^{-5}T^2 - 0.296 \times 10^{-8}T^3 + 0.807 \times 10^{-12}T^4) & \text{if } 300 < T[K] < 1000, \\ R_{H_2O}(0.271 \times 10^1 + 0.294 \times 10^{-2}T - 0.802 \times 10^{-6}T^2 + 0.102 \times 10^{-9}T^3 + 0.484 \times 10^{-14}T^4) & \text{if } 1000 < T[K] < 5000. \end{cases}$$

$$c_{p,N_2} = \begin{cases} \begin{aligned} &R_{N_2}(0.367 \times 10^1 - 0.120 \times 10^{-2}T \\ &+ 0.232 \times 10^{-5}T^2 - 0.632 \times 10^{-9}T^3 \\ &\quad - 0.225 \times 10^{-12}T^4) \end{aligned} & \text{if } 300 < T[K] < 1000, \\ \begin{aligned} &R_{N_2}(0.289 \times 10^1 + 0.151 \times 10^{-2}T \\ &- 0.572 \times 10^{-6}T^2 + 0.998 \times 10^{-10}T^3 \\ &\quad - 0.652 \times 10^{-14}T^4) \end{aligned} & \text{if } 1000 < T[K] < 5000. \end{cases}$$

Finally, the specific heat at constant volume is obtained from the following relation,

$$c_{v,i}(T) = \frac{c_{p,i}(T)}{c_{p,i}(T) - R_i} \quad (4.11)$$

To calculate the specific heats, c_p and c_v , of the gas at any point in the cylinder, one should know how much of the total gas is burned gases. Thus, the burned gas fraction is an important parameter and is defined as the burned gas mass divided by the total gas mass in the cylinder at any time instant. This implies that the burned gas fraction is highly influenced by the amount of fresh charge, the dominant fraction of total in-cylinder gas mass, and is not constant during the working cycle. For instance, c_p of the gas at EVC differs from that at IVC since in the latter point, the fresh charge is added to the residual gases. Furthermore, when the engine works under lean condition, burned gas fraction is lowered within higher λ . In general, the burned gas fraction, denoted by x_b , can be obtained from the following equation,

$$x_b = \frac{m_b}{m_{tot}} \quad (4.12)$$

Right after combustion completes until the exhaust valve opens, $x_{b,res}$ can be obtained from the following equation,

$$x_{b,res} = \frac{(AF)s + 1}{\lambda(AF)s + 1} \quad (4.13)$$

It is assumed that the gas composition is well-mixed after combustion so that when the exhaust valve opens, the burned gas fraction remains unchanged and therefore, the aforementioned equation is valid until the intake valve opens. However, when the intake valve opens, this assumption is not valid anymore since the fresh charge is added to engine cylinder and this influences the burned gas fraction considerably. In this case, one should first calculate the amount of burned gas at the instant of exhaust valve closing as below,

$$m_b = x_{b,res}m_{EVC} \quad (4.14)$$

This value can be used to calculate the burned gas fraction when the intake valve closes as shown below,

$$x_{b,IVC} = \frac{m_b}{m_{IVC}} \quad (4.15)$$

Finally, $c_{p,EVC}$ and $c_{p,IVC}$ can be obtained from the equations stated below,

$$c_{p,EVC} = x_{b,res}c_{p,b} + (1 - x_{b,res})c_{p,air} \quad (4.16)$$

$$c_{p,IVC} = x_{b,IVC}c_{p,b} + (1 - x_{b,IVC})c_{p,air} \quad (4.17)$$

4.7 Residual Gas Mass

It is assumed that the exhaust temperature is propagated from the exhaust manifold to the engine cylinder such that the temperature at EVC equals the temperature in the exhaust manifold, the residual gas mass can be obtained from the following equation,

$$m_{EVC} = \frac{p_{EVC}V_{EVC}}{R_{EVC}T_{em}} \quad (4.18)$$

However, the pressure in the exhaust manifold differs with that of the cylinder gas at the instant of EVC. This implies that the aforementioned assumption, $T_{em} = T_{EVC}$, should be modified to better predict the residual gas mass. The temperature at EVC can be estimated from the following equation,

$$T_{EVC} = T_{em} \left(\frac{p_{em}}{p_{EVC}} \right)^{\frac{1-\gamma}{\gamma}} \quad (4.19)$$

where γ is the heat capacity ratio of residual gas at T_{EVC} . Since this temperature is still unknown, γ can be approximated at T_{em} for the initial guess. To avoid making any assumption at this step, an iterative method is needed to adjust γ and T_{EVC} until a certain level of convergence is reached. The output of this iterative method is the T_{EVC} , its corresponding γ and residual gas mass.

According to equation (4.19), if p_{EVC} is lower than p_{em} , T_{EVC} is lower than T_{em} and vice versa. Therefore, if one uses T_{em} instead of T_{EVC} , the residual gas mass is under-estimated when p_{EVC} is lower than p_{em} and over-estimated when p_{EVC} is higher than p_{em} .

Besides, note that equation (4.18) is only valid when no valve overlapping occurs and a special consideration should be done when blow-by, or positive valve overlapping, happens.

4.8 Heat Transfer Model

Since the heat transfer during the gas exchange process is of interest, there is no need to study the burned and un-burned zones separately so that a single zone model is sufficient [18]. However, the heat transfer is divided into two parts, one

is to simulate the heat transfer of residual gases from EVC to IVC and the second is the heat transfer of the fresh air from IVO to IVC.

The heat transfer is modeled using instantaneous spatially-averaged Woschni correlation both for the residual and fresh charge gases with some minor modifications. Instead of using the instantaneous properties of the gas, their mean properties are used to obtain the average heat transfer coefficient. To get the total heat transfer over each cycle, the instantaneous heat transfer coefficient must be integrated over time. To do so, equation (3.31) must be divided by the engine speed which can be substituted by the following equation,

$$Ne = \frac{60V_{mp}}{2L} \quad (4.20)$$

where Ne is the engine speed in revolutions per minute, V_{mp} is the mean piston speed in meter per second and L is the stroke length. Accordingly, the average heat transfer coefficient can be obtained from the following equation,

$$dh_{mean} = CLB^{-0.2}p^{0.8}V_{mp}^{-0.2}T^{-0.546} \quad (4.21)$$

This equation is valid for both components, the fresh air and the residual gases. Note that B is the cylinder bore and p and T are the mean pressure and temperature of the gas, respectively. Besides, the model tuning, C , is found using a non-linear least square curve fitting to the errors in the air mass estimation. Determining the temperature of the fresh charge and residual gas after the heat transfer, it is time to mix the two gases together until they build a homogeneous content.

4.9 Total In-Cylinder Trapped Gas Mass

According to the Δp method, shown in equation (3.5), the temperature at the initial point must be known. Accurate estimation of this temperature is challenging since it is dependent on the heat transfer and pressure rise from IVC to the initial point, which are both related to the operating condition [2]. To determine this temperature, the following steps have been performed.

When intake valve opens, the mixing and heat transfer is done concurrently. To simplify these two processes, it is assumed that the entire mixing occurs at IVC. At this time, the balance of energy can be written as,

$$m_{IVC}c_{v,IVC}T_{IVC} = m_{air}c_{v,air}T_{air} + m_{EVC}c_{v,res}T_{res} \quad (4.22)$$

where the temperatures T_{air} and T_{res} are those after heat transfer is completed. Since the aim is to calculate T_{IVC} from the above-mentioned equation, both sides of this equation is divided by $m_{IVC}c_{v,IVC}$. Additionally, m_{air} can be substituted from the following equation,

$$m_{air} = m_{IVC} - m_{EVC} \quad (4.23)$$

As discussed in section 4.5 by equation (4.13), the residual gases are composed of the burned gas and air. Having said that, m_{air} represents for the fresh charge entering the cylinder during the intake stroke. Finally, m_{IVC} can be written as below,

$$m_{IVC} = \frac{p_{IVC} V_{IVC}}{R_{IVC} T_{IVC}} \quad (4.24)$$

Insertion of m_{air} and m_{IVC} from equations (4.23) and (4.24) into equation (4.22) and rearrangement of the resultant equation yields,

$$T_{IVC} = T_{air} \frac{c_{v,air}}{c_{v,IVC}} + \frac{m_{EVC} R_{IVC} T_{IVC}}{p_{IVC} V_{IVC}} \left(\frac{c_{v,res} T_{res}}{c_{v,IVC}} - \frac{T_{air} c_{v,air}}{c_{v,IVC}} \right) \quad (4.25)$$

As mentioned previously, all the temperatures in equation (4.25) are those after the heat transfer is completed So that T_{res} differs from T_{EVC} and T_{air} is not the same as that in the intake manifold.

It is also important to note that to use the equation (4.25) for the first try, special consideration is needed because $c_{v,IVC}$ cannot be quantified accurately at this step since the mass of air sucked into the cylinder during the intake stroke is unknown and more importantly, T_{IVC} is presented in both sides of the equation.

One solution is to conduct an iterative method and replace $\frac{c_{v,IVC}}{c_{v,air}}$ with one in the first iteration and make initial guess for the temperature at IVC . The second alternative is to use the following equation for the total gas mass at IVC ,

$$m_{IVC} = \frac{p_{IVC} V_{IVC}}{R_{air} T_{im}} \quad (4.26)$$

From this equation, the air mass is the difference between the total mass and the residual gas mass. Consequently, the burned gas fraction at IVC can be calculated and the temperature at IVC can be obtained from the following simplified equation,

$$T_{IVC} = T_{EVC} x_{b,IVC} + T_{im} (1 - x_{b,IVC}) \quad (4.27)$$

This temperature can be used in Δp method to obtain the total mass in the cylinder. Subsequently, fresh charge mass can be computed by subtracting the residual gases mass from the total trapped gas mass. This mass of air can be used to estimate $c_{v,IVC}$ in the second iteration. This iterative method can be continued until a desirable level of convergence is reached. At the end, the temperature at the intake valve closing, the total mass trapped in the cylinder and the mass of fresh charge are obtained.

Another challenge in this step is the selection of points a and b for the Δp interval. Previous works and some preliminary investigations in this master thesis have shown that moving the point b towards TDC can give a better accuracy in the total mass estimation and lower the sensitivity of the method to points a and b ; however, the probability of interfering with the fuel injection time gets higher [2]. If point a gets close to the IVC, the accuracy of the method decreases due to

the wave effects of the intake process and the uncertainty in the actual time of intake valve closing [2].

In this study, two intervals are examined, one is from *IVC* to 70° BTDC and the second interval is from 70° to 50° BTDC. Moreover, to obtain the polytropic coefficient, a polytropic relationship between the pressure and volume of cylinder is considered as shown below,

$$pV^k = \text{constant} \quad (4.28)$$

Taking the logarithm from both sides of this equation yields,

$$\log(p) + k\log(V) = \log(c) \quad (4.29)$$

Equation (4.29) in the vector-matrix fashion can be written as below,

$$\begin{bmatrix} \log(V_1) & -1 \\ \log(V_2) & -1 \\ \vdots & \vdots \\ \log(V_n) & -1 \end{bmatrix} \times \begin{bmatrix} k \\ \log(c) \end{bmatrix} = \begin{bmatrix} -\log(p_1) \\ -\log(p_2) \\ \vdots \\ -\log(p_n) \end{bmatrix} \quad (4.30)$$

which is equivalent to,

$$Ax = b \quad (4.31)$$

where A and b are the non-square matrices and x is the unknown vector. To compute x , both sides of equation (4.31) can be multiplied by transpose of matrix A as following,

$$A^T Ax = A^T b \quad (4.32)$$

where $A^T A$ is a square matrix and possibly invertible; therefore, x is computed from the following equation,

$$x = (A^T A)^{-1} A^T b \quad (4.33)$$

Finally, the first element in the vector x is the polytropic index during compression.

4.10 Cylinder Wall Temperature

Both methods explained in the previous chapter, section 3.3, were investigated in this master thesis. The second method, indicated by equation (3.39) was found more reliable in a wide range of operating conditions. The first method mostly gives cylinder wall temperature lower than the coolant temperature which is not physically possible. According to this finding, the following equation is implemented for estimation of cylinder wall temperature,

$$T_w = c_0 + c_1 Ne + c_2 Tq \quad (4.34)$$

As it is indicated, there is a linear dependency of cylinder wall temperature on the engine speed and the engine torque.

4.11 Temperature at 70° BTDC

As stated previously in this chapter, two intervals are investigated for examining Δp method. The first interval, which is selected from IVC to 70° BTDC, uses the temperature at IVC based on equation (3.5). This temperature is estimated according to the method explained in section 4.9. However, the second interval is selected from 70° until 50° BTDC, where the temperature at 70° BTDC must be determined. This temperature can be calculated in three different ways.

The first method is based on a polytropic compression from IVC to 70° BTDC according to the following equation,

$$T_{-70} = T_{IVC} \left(\frac{V_{IVC}}{V_{-70}} \right)^{(k-1)} \quad (4.35)$$

where k is the polytropic index and can be computed from equation (4.30) using the measured cylinder pressure and volume from IVC to 70° BTDC. An alternative is to use the ideal gas law to compute the temperature change from IVC to 70° BTDC as indicated below,

$$\Delta T = \frac{p_{-70} V_{-70} - p_{IVC} V_{IVC}}{m_{IVC} R_{IVC}} \quad (4.36)$$

and,

$$T_{-70} = T_{IVC} + \Delta T \quad (4.37)$$

The last suggestion is to make an average of the two aforementioned methods.

4.12 Cycles With Positive Valve Overlap

As mentioned previously in this chapter, the second assumption stated in section 4.4 becomes invalid for the cycles with positive valve overlap. In these cycles, scavenging or back-flow influences the gas composition from IVO to EVC and their effect may not be negligible. Therefore, ideal gas constant and specific heat in constant pressure and volume vary from the start until end of valve overlap. The burned gas fraction also changes during the valve overlap since neither the composition of the gas nor the amount of total gas in the cylinder remains constant. In such cases, the burned gas fraction should be estimated differently since λ is affected by the scavenged gas and is not the representative of the gas composition right after combustion completes.

Regarding the experimental data, the mass air flow meter mounted in the intake manifold does not measure the air mass trapped the engine cylinder since this mass might travel directly into the exhaust manifold.

In overall, additional model is required to model the gas mass that travels through either of the valves during the valve overlap. This mass can be the scavenging of fresh charge or back-flow of the exhaust gas. To measure this mass, the timing of intake and exhaust valves are essential factors [17]. Overlap Factor (OF) defines the magnitude of valve overlap according to the following equation,

$$OF = \int_{IVO}^{IV=EV} A_{int} d\theta + \int_{IV=EV}^{IVC} A_{exh} d\theta \quad (4.38)$$

where A_{int} and A_{exh} are the effective opening areas of the intake and exhaust valves, respectively. $IV=EV$ denotes for the crank angle at which the intake valve opening area equals to the exhaust valve opening area. The figure below demonstrates an example of intake and exhaust effective valve areas.

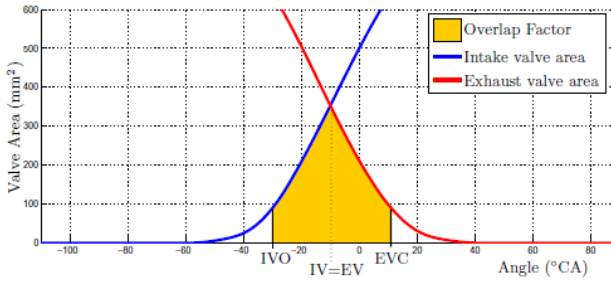


Figure 4.2: Overlap Factor [17]

The OF together with the conditions at intake and exhaust manifold and engine speed determine the degree of scavenging or back-flow.

5

Results and Discussion

Before presenting any result, it is more convenient to indicate, characterize and name the studied tests as shown in the following table.

Table 5.1: A Complete Set of Tests

Test Number	Operating Condition		Cam Phasing
	Engine Speed [rpm]	Engine Torque [Nm]	[Intake; Exuast] [CAD]
1	1200.0430	2464.1250	[0, 0]
2	1200.0670	2464.1320	[0, 0]
3	1200.0510	560.5019	[0, 0]
4	1200.0570	1163.7790	[0, 0]
5	1200.0490	1753.8040	[0, 0]
6	1200.0730	362.1437	[15, -15]
7	1200.0650	162.4362	[15, -15]
8	1800.0200	317.3793	[15, -15]
9	1200.0570	163.5386	[30, -30]
10	1200.0610	363.9020	[30, -30]
11	1800.0280	319.8585	[30, -30]
12	1200.0660	164.1016	[45, -45]

As it is evident, two engine speeds, 1200 and 1800 rpm have been investigated together with a wide range of engine torques, covering the low-load operating conditions such as the tests 7, 9 and 12 to the high-load cases such as the tests 1,

2 and 5. Also, various symmetric intake and exhaust cam phasings are analyzed. The positive values shown in last column of table 5.1 are referred to as the late valve events, when compared to the cycles with the nominal valve events, and the negative values stand for the early valve events. Thus, the intake valve is typically opened and closed late while the exhaust valve is opened and closed early. Lastly, the other recorded experimental data are listed in table 5.2.

Table 5.2: Other Experimental Data

Test Number	Intake Manifold		Exhaust Manifold		Coolant Temperature	Lambda	\dot{m}_{air}
	Pressure	Temperature	Pressure	Temperature			
	[kPa]	[K]	[kPa]	[K]	[K]	[-]	[g/s]
1	316.2375	304.9772	276.8005	773.9854	362.8984	1.8252	69.9115
2	289.5136	303.5989	249.9209	742.1706	362.8175	1.7066	63.0970
3	134.1495	301.7718	134.8955	541.3159	362.9136	2.9581	29.0382
4	172.5897	301.3046	158.2876	630.0424	362.9158	2.0729	37.4630
5	217.2658	301.9391	189.9173	675.5197	362.8508	1.7882	46.9722
6	127.7021	305.3910	125.4718	515.3054	363.1999	3.5082	25.0644
7	120.4159	305.6108	121.8454	457.4648	362.8722	5.1491	23.3166
8	160.5840	305.6379	165.1085	520.1937	362.9640	3.9781	46.7015
9	115.7748	311.3936	114.4464	505.9361	363.1540	3.8479	18.0228
10	122.8459	311.2487	117.4254	578.1778	363.1500	2.6417	19.5777
11	108.4183	309.9792	112.8300	650.9227	363.2034	2.2035	26.1392
12	116.3556	321.1160	111.2568	572.4808	363.1554	2.8417	14.1876

As mentioned before, the pressure trace, the intake and exhaust manifold temperature and pressure, coolant temperature, λ and mass air flow rate in the intake manifold are measured for each test. It is important to note that the coolant temperature is measured before and after absorbing heat from the cylinders while the values indicated in the table above are those after the heat is transferred to the coolant.

It can be seen from table 5.2 that even-though the intake manifold temperature varies slightly among the tests, the exhaust manifold temperature changes largely. This is due to the fact that the boost condition is only dependent on the atmospheric temperature/pressure and turbocharger characteristics while the exhaust condition is highly influenced by the previous combustion and mean temperature of the gas which are largely varying by operating conditions. Having said that, test 12 is an exception since the intake manifold temperature is relatively higher than that in the other tests; in this test, the exhaust valve opens and closes 45° earlier than normal; this means that more residual gases are trapped and re-compressed after EVC. Therefore, when the intake valve opens, the residual gas mass with high pressure and temperature travels from the engine cylinder into the intake port, mixing with the fresh air and increasing the temperature in

the intake manifold.

The coolant temperature stands relatively constant at 363K with a slight variation among the tests. Also note that \dot{m}_{air} indicated in table 5.2 is the mass air flow rate per each engine cylinder.

Additionally, since the same fuel is used for all the tests, the higher lambda value, the higher amount of air mass measured during the experimental phase. Last but not least, the amount of air that flows in the intake port is the same as that trapped the cylinder during the intake stroke since there is a negative valve overlap in all the tests.

To compute the total amount of air entering the cylinder in each cycle, the following equation is used,

$$m_{air} = \frac{2\pi n_r \dot{m}_{air}}{N_e} \quad (5.1)$$

where n_r is 2 for the four-stroke engines, as mentioned in chapter 3. Equation (5.1) gives the measured mass of air because the air mass flow rate is obtained from measurements.

Note that each test itself includes a number of tests with a slight change in the operating conditions and in total, 60 cycles are investigated. However, to emphasize on the most important findings, only the results of some of the tests are presented in this chapter and the reader is referred to Appendix B for the complete set of results of all the studied tests.

5.1 Experimental Data

At the very early stage of this study, the outputs from experiment are visualized and the results are indicated in figure 5.1.

The first plot in this figure demonstrates the pressure curve as a function of crank angle. This pressure curve is averaged over approximately 50 cycles and it can be clearly seen that the pressure during combustion and at the late phase of compression strokes is substantially larger than that during the intake and exhaust strokes.

The second plot indicates the low pressure zoom of the first plot together with the time-averaged intake and exhaust manifold pressures. This plot provides some information about the flow direction from the cylinder to the manifolds and vice versa. For instance, if the cylinder pressure is lower than the intake manifold pressure, the flow travels from the cylinder into the intake manifold while the intake valve is open.

The third and fourth plots displays the p-V, or indicator, diagram and cylinder volume resolved by the crank angle, respectively. Finally, the fifth plot reveals the intake and exhaust valve lift profiles after considering the influence of valve lash. Based on the discussion in section 4.12, this plot determines the magnitude of OF in the engine cycles with positive valve overlap. This value together with the relation among the intake, exhaust and cylinder pressure assesses the gas flow direction during the valve overlap and appoints if any back-flow or scavenging

happens. Identifying mass distribution, a better model of heat transfer can be performed.

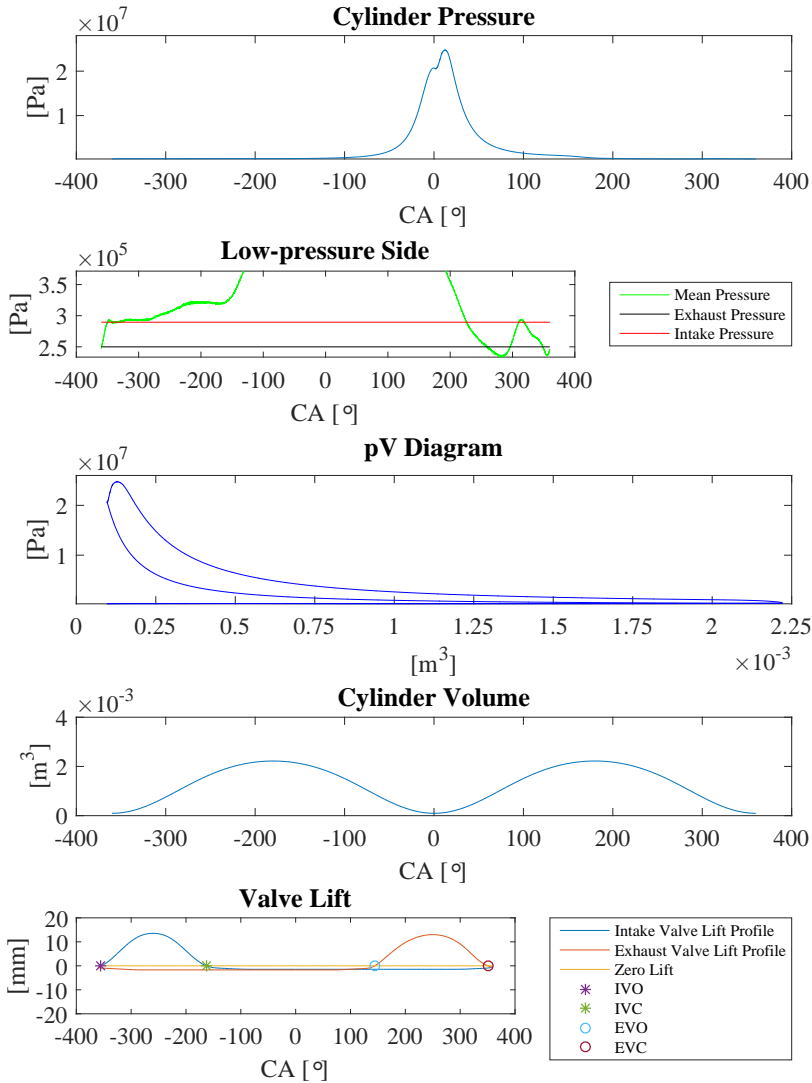


Figure 5.1: Experimental Data and Demonstration of Pressure Trace, Indicator Diagram, Cylinder Volume and Valve Events for Test 2

Additionally, the magnitude of peak cylinder pressure is dependent on the operating condition and torque request while its position is dependent on the fuel injection time. These phenomena are demonstrated in figure 5.2, in which the pressure trace of all the 12 examined tests are shown.

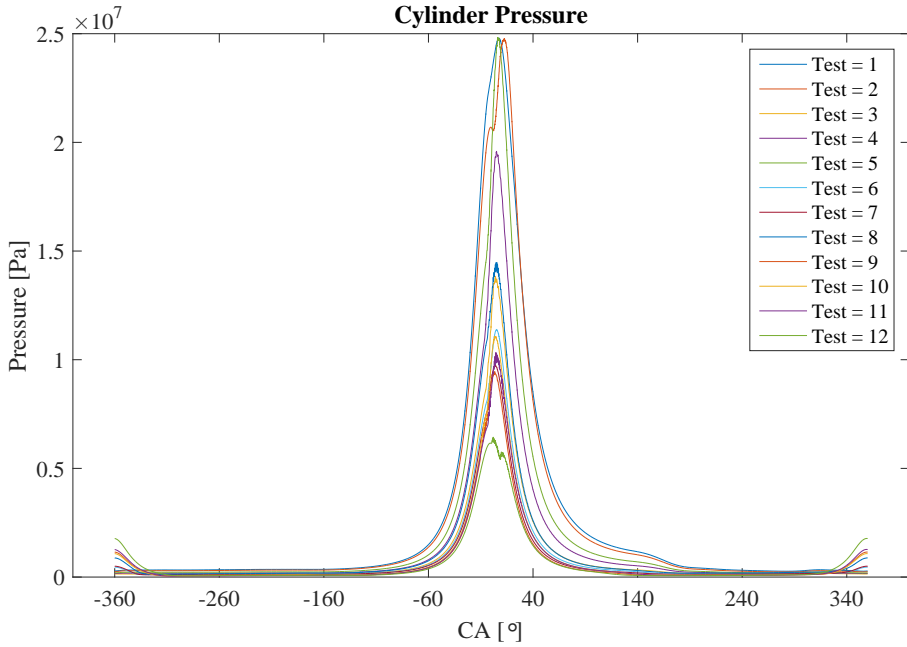


Figure 5.2: Cylinder pressure trace for all the 12 Tests

Considering the first and last plot in figure 5.1, the cylinder pressure and cylinder volume when valve events happen can be obtained. Tables 5.3 and 5.4 summarize the in-cylinder pressure and volume at IVO, IVC, EVO and EVC.

Table 5.3: Volume at the Opening and Closing of Intake and Exhaust Valves

Test Number	V_{IVO}	V_{IVC}	V_{EVO}	V_{EVC}
	[L]	[L]	[L]	[L]
1	0.1025	2.1874	2.0779	0.1169
2	0.1025	2.1874	2.0779	0.1169
3	0.1025	2.1874	2.0779	0.1169
4	0.1025	2.1874	2.0779	0.1169
5	0.1025	2.1874	2.0779	0.1169
6	0.1826	2.1046	1.9322	0.2239
7	0.1826	2.1046	1.9322	0.2239
8	0.1826	2.1046	1.9322	0.2239
9	0.3479	1.9708	1.7367	0.4115
10	0.3479	1.9708	1.7367	0.4115
11	0.3479	1.9708	1.7367	0.4115
12	0.5802	1.7866	1.4963	0.6594

Table 5.4: Pressure at the Opening and Closing of Intake and Exhaust Valves

Test Number	<i>PIVO</i>	<i>PIVC</i>	<i>PEVO</i>	<i>PEVC</i>
	[kPa]	[kPa]	[kPa]	[kPa]
1	266.5343	315.5803	1084.8910	240.0704
2	242.1418	290.6017	954.3026	212.3063
3	130.7678	134.1567	303.5499	138.4930
4	159.4059	173.1265	483.2966	152.7873
5	189.8300	218.2347	650.4872	170.4631
6	136.1273	130.6067	272.6716	170.3414
7	149.0345	123.5706	211.4204	177.5874
8	271.5619	163.7019	319.1515	289.7227
9	169.6438	114.6138	224.0623	178.5535
10	160.3805	121.9128	284.0463	173.0444
11	189.9538	114.7839	283.5926	192.8096
12	132.8442	116.0474	264.8685	152.0443

The four pressures presented in table 5.4 are both dependent on the cylinder volume and cylinder gas mass. During the intake stroke, the cylinder volume increases meanwhile the air is entering the cylinder. In high-load tests, i.e. tests 1 and 2, runners and throttle become less restrictive to allow a higher amount of fresh air entering the cylinder and to produce more power. This large air mass compensates for the influence of volume increase such that the cylinder pressure increases from IVO to IVC. In contrast, the pressure decreases during the intake stroke in low-load tests and this is due to the fact that less amount of fresh air enters the cylinder in these tests. This phenomenon is addressed later in this chapter when the results of estimated air for each test are presented.

It can be seen from table 5.4 that the cylinder pressure at EVC is well-below that at EVO for all the tests. The high load tests generate higher pressures during the combustion stroke and the subsequent result is the higher pressures at EVO. This effect is even more pronounced when the exhaust valve opens earlier than normal. The opposite situation happens either when the torque requested from the engine is low or the exhaust valve opens with delay.

5.2 Pressure Pegging

As explained in the previous chapter, pressure pegging is essential to obtain the correct/absolute pressure at any crank angle/time. In this study, the intake manifold pressure referencing method is implemented to the raw measured pressure signals and the figure below illustrates both the experimental and corrected pressure curves over the entire working cycle.

As can be clearly seen, the pressure correction has a large influence on the pressures in the intake and exhaust strokes compared to those in the compression and combustion strokes.

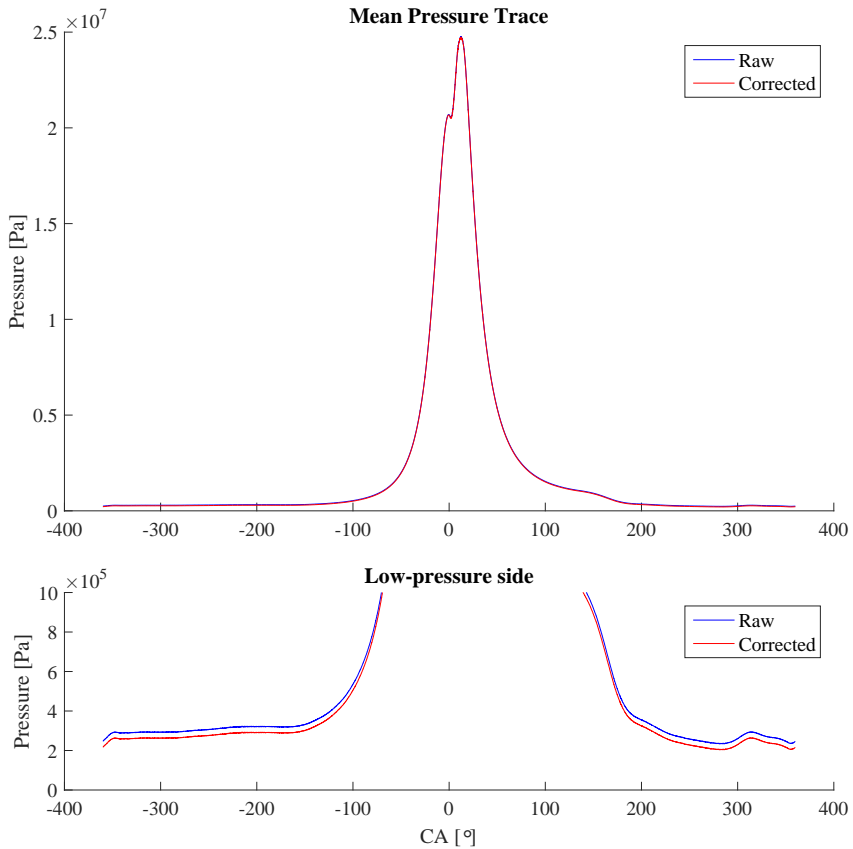


Figure 5.3: Raw versus Corrected Cylinder Pressure Trace for Test 2

5.3 Total Gas, Fresh Air and Residual Gas Mass

The aim in this section is to present the total estimated gas mass in the cylinder and its composition. Since the results of mass estimation determine whether the purpose of this master thesis is fulfilled or not, a complete set of results is shown in table 5.5.

As stated earlier, the total and residual gas masses are modeled on a thermodynamic basis and the difference between them determines the fresh air entering the cylinder in each operating cycle. This air mass is a factor of how precise the model is since the estimated air mass is compared with that obtained by measurement.

It is also important to mention that all the errors shown in table 5.5 are the

relative errors and are generally obtained from the following equation,

$$Error\% = \frac{Theoretical - Experimental}{Experimental} \times 100 \quad (5.2)$$

The total in-cylinder gas mass is estimated by five different approaches. The first approach applies the ideal gas law at intake valve closing. The second alternative implements the Δp method between intake valve closing and 70° BTDC. The three last approaches apply the Δp method from 70° to 50° BTDC while the initial temperature is obtained in three different ways following the method explained in section 4.11.

The results shown in this section are the average over the five aforementioned ways and a more detailed set of results are presented in Appendix B. The beneficial feature of calculating the mean error is that the error can be reduced when the air is under-estimated by some alternatives and over-estimated by others. In another words, the deficiencies of an alternative are lowered and the predicted air mass is closer to the reality.

Table 5.5: Total Gas, Fresh Air and Residual Gas Mass

Test Number	Estimated			Measured	Error in Air Estimation
	m_{tot}	m_{res}	m_{air}	m_{air}	
	[gr]	[gr]	[gr]	[gr]	%
1	6.9763	0.1308	6.8455	6.9909	-2.0795
2	6.4080	0.1213	6.2867	6.3094	-0.3583
3	3.0112	0.1032	2.9080	2.9037	0.1481
4	3.8666	0.0995	3.7670	3.7461	0.5580
5	4.8453	0.1055	4.7398	4.6970	0.9106
6	2.7587	0.2370	2.5217	2.5063	0.6152
7	2.6305	0.2724	2.3581	2.3315	1.1394
8	3.4184	0.3731	3.0453	3.1134	-2.1874
9	2.2416	0.4480	1.7936	1.8022	-0.4793
10	2.3497	0.3871	1.9625	1.9571	0.2484
11	2.1093	0.3705	1.7388	1.7426	-0.2172
12	1.9841	0.5610	1.4231	1.4187	0.3140

In general, the operating condition defines how much air is needed for the next cycle to generate the requested torque at the wheel to be able to run the vehicle forward. According to table 5.5, tests 1, 2 and 5 demand the highest torques from the engine; therefore, the highest amount of air is estimated in these tests.

Moreover, the earlier the exhaust valve closes, the more residual gases are trapped in the engine cylinder and vice versa. This statement is in complete agreement with the results indicated in table 5.5. Test 1 with the latest exhaust valve closing has the lowest amount of residual gas while test 12 with the earliest exhaust valve closing traps the highest amount of residual gas mass and the former is five times smaller than the latter. The finding here is that the cam phasing controls the amount of residual gas mass considerably.

It can be also seen from table 5.5 that the magnitude of the fresh air is much larger than that of the residual gas. Therefore, the former has a larger impact on the amount of total mass than the latter. This explains why test 1 with the highest amount of air has the highest amount of total gas mass and test 12 with the lowest amount of air has the lowest amount of total gas mass.

The negative values in the air estimation error refer to the under-estimation of air mass by the model while the positive values show the over-estimation. More importantly, the relative error between the estimated and measured air mass is well-below 1% in average, being around 1% in one of the tests and reaches the maximum of 2% in two of them.

It is also important to note that the reason for getting high error, around 2% in two of the tests, is due to the fact that the error in all the above-mentioned approaches have the same sign for these tests and could not help to lower the average error. Finally, it is worth mentioning that this model works properly for the cycles with symmetric cam phasing and negative valve overlap. A special consideration needs to be taken for the tests with asymmetric cam phasing or with positive valve overlap.

5.4 Composition Fraction

As mentioned in chapter 4, the burned gas fraction is not constant over the entire working cycle due to the fact that the amount of the burned gas and the total in-cylinder gas mass vary over the working cycle. To be precise, the burned gas fraction has its minimum value at the start of combustion and increases to a relatively large value when combustion completes. This value, then, remains constant until the exhaust valve opens since neither the burned gas nor the total mass in the cylinder changes. Under the second assumption stated in the previous chapter, the gas composition remains unchanged from EVO to EVC which means both the exhaust gas and the in-cylinder gas have the same composition. Consequently, the burned gas fraction from the completion of combustion until IVO is constant and called the burned gas fraction in the residual gas. From IVO until IVC, the fresh charge enters the cylinder; accordingly, the burned gas fraction decreases due to the increase of the total mass. Finally, this value remains constant until the next combustion initiates and is called the burned gas fraction after IVC.

According to the explanation above, two burned gas fractions, $x_{b,res}$ and $x_{b,IVC}$, are presented in table 5.6. The former corresponds to the burned gas fraction before intake valve opens and the latter is that after IVC.

Table 5.6: Composition Fraction

Test Number	m_{air}	λ	$x_{b,res}$	$x_{b,IVC}$
	[gr]	[-]	%	%
1	6.85	1.8252	56.4336	1.0527
3	2.9080	2.9581	35.3134	1.2077
6	2.5217	3.5082	29.8821	2.5566
8	3.0453	3.9781	26.4131	2.8626
9	1.7936	3.8479	27.2906	5.4206
11	1.7388	2.2035	47.0400	8.1782
12	1.4231	2.8417	36.7252	10.3596

According to equation (4.13), the burned gas fraction in the residual gas mass is inversely proportional to the air to fuel equivalence ratio, λ . Therefore, in test 8 with the highest λ , the burned gas fraction in the residual gas is the lowest. In contrast, test 1 with the lowest λ has the highest burned gas fraction in the residual gas mass. Furthermore, the burned gas fraction after intake valve closes is not only dependent on λ , but also on the total air sucked into the cylinder during the next intake stroke. This implies that the more air entering the cylinder, the larger amount of total mass in the cylinder and the lower burned gas fraction after intake valve closes.

Note that neither the burned gas fractions during combustion propagation, nor that during the intake stroke are evaluated in this study.

5.5 Estimation of Temperatures

The cylinder wall temperature and the temperature at IVC are of high importance in this model since they determine the magnitude of heat transfer during the gas exchange process and the amount of total gas mass in the cylinder after IVC.

This section is devoted to the results predicted for these two temperatures together with some other influential temperatures such as the temperature at exhaust valve closing. Table 5.7 demonstrates the temperatures predicted by the model together with some measured data.

Since the heat transfer is taken into account, the air temperature differs with the intake manifold temperature. The same argumentation holds for the difference between the temperature of residual gas and exhaust valve closing temperature. Based on equation (4.25), the intake valve closing temperature is linearly dependent on T_{air} and T_{res} . However, table 5.7 shows that this temperature is much more influenced by the temperature of fresh charge than that of the residual gas. This is because the air mass is much larger than the residual gas mass, see table 5.5. Moreover, the conservation of energy states that the intake valve

Table 5.7: Measured and Estimated Temperatures

Test Number	Measured		Estimated				
	T_{im}	T_{em}	T_{air}	T_{res}	T_{EVC}	T_{IVC}	T_w
	[K]	[K]	[K]	[K]	[K]	[K]	[K]
1	304.9772	773.9854	335.6770	612.3710	746.9085	341.6843	407.8131
3	301.7718	541.3159	332.5110	462.0917	545.1425	337.3700	387.3356
6	305.3910	515.3054	339.0534	382.5852	559.3024	344.3094	385.2022
8	305.6379	520.1937	339.9255	382.7739	604.1282	347.2516	395.5823
9	311.3936	505.9361	346.6537	327.5888	569.9658	347.5436	383.0655
11	309.9792	650.9227	354.6927	389.7191	745.1835	368.4801	395.6091
12	321.1160	572.4804	359.9937	334.1984	621.4080	361.9051	383.0717

closing temperature must be between the temperature of fresh charge and that of residual gases. This is in complete agreement with the results shown in table 5.7.

As explained in the previous chapter, the cylinder wall temperature is estimated from the following equation,

$$T_{CylWall} = c_0 + c_1 \frac{Ne}{1000} + c_2 \frac{Tq}{1000} \quad (5.3)$$

where Ne , the engine speed, is given in revolution per minute and Tq , the engine torque, is given in Nm . The three constants in equation (5.3) are calculated by running an optimization such that the air mass error is minimized.

As shown in Appendix B, each test itself consists of several tests. The first experiment in each test is used for the determination of model constants through optimization and the remaining tests are used for model validation. As a result of this optimization, the three constants used in equation (5.3) are 359.5800, 18.1043 and 10.7572, respectively.

As expected, the cylinder wall temperature is always higher than the coolant temperature and is varying between 383 and 407K. The highest and lowest cylinder wall temperatures are recorded for test 1 and 9 with the highest and lowest torques, respectively.

A detailed validation of the results for the estimated temperatures is not possible in this study since neither of the temperatures are measured in this study. However, since the cylinder wall temperature is used to estimate the total in-cylinder gas mass, the results are implicitly validated.

To validate the estimated temperatures independent of the validation of the estimated masses, a simple way is to accept the results as soon as the cylinder wall temperature is higher than the coolant temperature. Another alternative is to roughly compare the estimated cylinder wall temperatures with the measured cylinder head temperatures. It is obvious that the cylinder head has always

higher temperature compared to the average cylinder wall temperature and the difference is mainly dependent on the combustion stroke, engine geometry and some other factors.

A measurement on the temperature of engine cylinder head was conducted at Scania in 2009. Each cylinder was equipped with three to eight temperature sensors located in the combustion chamber, two other sensors measuring the coolant temperature as well as a sensor for the in-cylinder pressure. The observation is that when the engine is running at 1200 rpm with nominal cam phasing and coolant temperature of 90° (363K), the cylinder head temperature is approximately 596K in cylinder 4 and 574K in cylinder 8 when the maximum pressure in the cylinder is approximately 200 bar.

Test 4 has a similar operating condition to the aforementioned part of measurement with a slightly different maximum pressure. The estimated cylinder wall temperature is approximately 394K, see Appendix B. The main difference between the measured values and the estimated temperature originate from the fact that the cylinder head is always hotter than the average cylinder wall temperature because of being closer to where the combustion initiates. Furthermore, the dissimilarities between the maximum in-cylinder pressures is another factor to cause differences between the aforementioned temperatures.

5.6 Pressure and Temperature Trace during Compression

As a measure of how precise the model can predict the properties of the gas in the cylinder, the pressure curve during the compression is estimated and compared with the experimentally obtained curve. Assuming a polytropic compression, the pressure at IVC can be estimated according to the following equation,

$$p_{IVC,est.} = \frac{c}{V_{IVC}^k} \quad (5.4)$$

where c and k can be computed from the experimental data according to equation (4.30). This pressure can be used for the estimation of the other pressures during the compression stroke, as indicated below,

$$p_{comp,est.} = p_{IVC,est.} \left(\frac{V_{IVC}}{V_{comp}} \right)^k \quad (5.5)$$

Another alternative is that any newly estimated pressure and its corresponding volume can be used in equation (5.5) instead of those at IVC. Applying the ideal gas law at any point during the compression gives the compression temperatures as indicated below,

$$T_{comp} = \frac{p_{comp} V_{comp}}{m_{IVC} R_{IVC}} \quad (5.6)$$

It is assumed that no mass leakage happens during the compression stroke so that the total mass in the cylinder is the same from IVC until fuel is injected. This assumption may become invalid at the later phase of compression due to high pressures in the cylinder and more possibility of mass leakage.

Figure 5.4 shows both the experimental and estimated pressure curves during the compression stroke for test 2. As can be seen in this figure, the predicted pressure curve is in a good agreement with the that obtained experimentally.

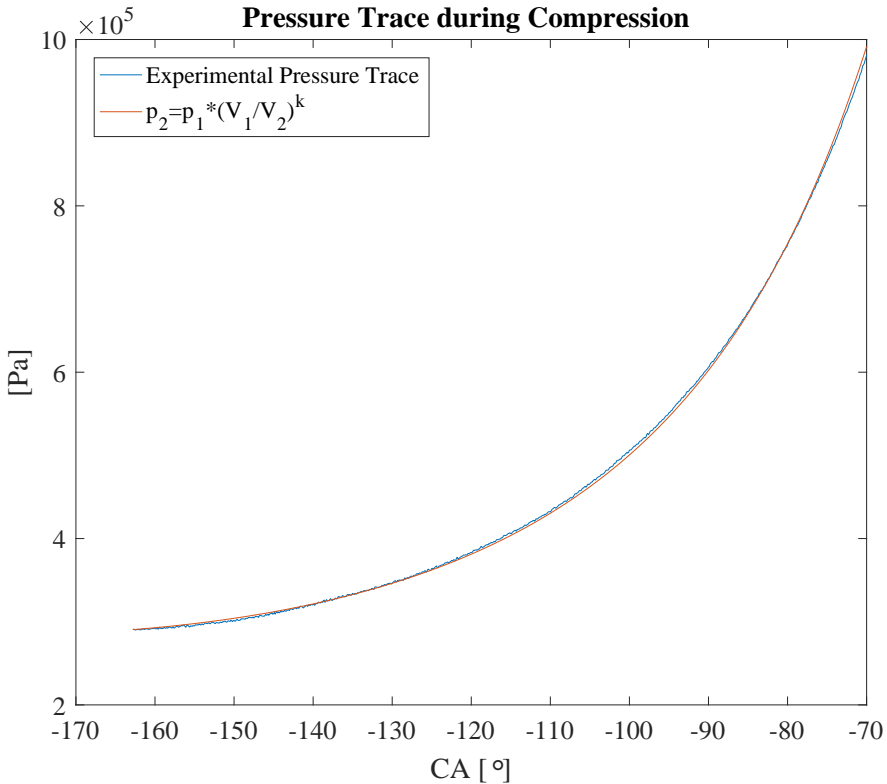


Figure 5.4: Measured and Predicted Pressure Curves during Compression for Test 2

Figure 5.5 indicates the temperature predicted during the compression stroke, for 4 tests, 1, 6, 9 and 12. Since no measurement is conducted for the temperatures in the cylinder, validation of results is not possible. However, since the masses and the temperatures in the cylinder are interconnected, and air estimation is validated for all the studied tests, the results seems to be reliable.

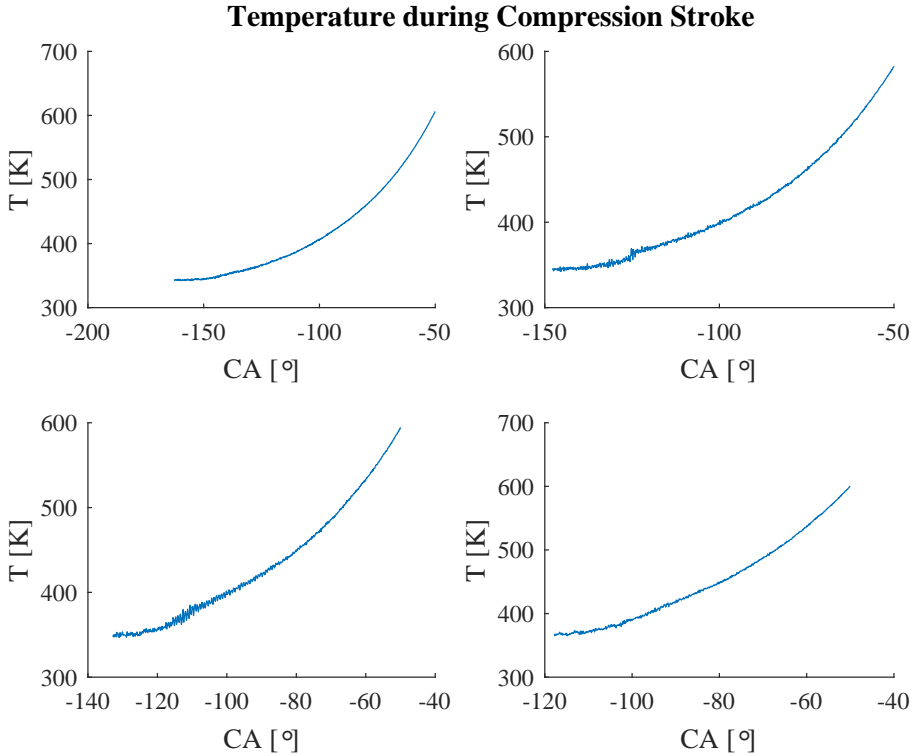


Figure 5.5: Predicted Temperature Curve during Compression for Tests 1, 6, 9 and 12

From Left to Right, Top: test 1 and 6 Down: 9 and 12

5.7 Other Findings

5.7.1 Computational Costs

Computational cost is generally influenced by the desirable level of accuracy, the number of iterative sub-models, if there exists any, and their level of convergence. In this study, the computational expenses can be studied from two perspectives, one is to conduct a comparison between the individual tests and to make a conclusion about the most computationally expensive test and the other is to consider the computational burden of the optimization process and investigate the influence of model constant on the computational time.

Based on the methodology explained in chapter 4, two iterative sub-models are used, one for the residual gas mass and the other for the total gas mass. Due to this reason, taking the computational expenses into account is found essential and the results are summarized in table 5.8.

Table 5.8: Computational Expenses for each Test

Test Number	Computational Time
	[sec.]
1	0.8944
2	0.4560
3	0.4064
4	0.4008
5	0.4059
6	0.3978
7	0.3908
8	0.3640
9	0.4762
10	0.4865
11	0.4789
12	0.4487

According to table 5.8, the execution time is well-below 1 second for all the tests and is fairly constant around 0.4 seconds except test 1. This test is about two time more computationally expensive than any other test. This issue can be addressed to the initialization time and the number of iterations required for a certain level of convergence. Regarding the initialization, it can be generally stated that memory pre-allocation can significantly speed up the execution time, especially when loops and/or vectors and matrices are used in the Matlab code. Vectorized operations, instead of for loops, can also increase the computational efficiency. Since this study has taken advantage of both aforementioned approaches, the differences in the computational expenses arise from another dissimilarity among the tests.

To find out why the first test is more numerically expensive than the others, the time dedicated for the initialization and pre-allocation is subtracted from the total computational time consumed by each test and the observation is that the first test is still the most computationally expensive test.

Further investigations confirm that the first test requires a longer time for computing the polytropic index, temperatures and pressures during the compression stroke. This issue can be addressed to the fact that this test with the earliest IVO, and subsequently the earliest IVC, has a larger region between IVC and 70° BTDC where the before-mentioned properties are determined. In another words, the first test deals with larger matrices compared to the other tests in its main loop. Additionally, the number of iterations differs slightly among the tests, mostly 10 iterations are needed in total if the convergence level for both loops is

set to $1e-5$.

Moreover, five model constants need to be optimized, two of them are used for the heat transfer and the other three ones for the estimation of the cylinder wall temperature. The observation is that the more constants to be optimized, the more computationally expensive the model becomes and the proportionality is non-linear. It is also found out that the computational time is largely dependent on the starting points and varies between 500 to up to 800 seconds, typically around 600 seconds. Another finding is that the higher convergence criteria in the model, the more computationally expensive the model becomes and vice versa.

Last but not least, the computational time for the optimization is significantly higher than that of the execution of each test. Therefore, one should compromise between computational expenses and the number of tests used for optimization, to quantify the model constants. Finding a suitable trade-off between the level of accuracy in the for-loops and the computational costs is also important.

5.7.2 Optimization Process

Regarding the optimization, it is important to make sure that a global minima is found. If the initial values are either the same as or close to the optimized constants, it is a clue that either the initial values are not selected correctly or a local minima is found instead of the global minima. An alternative to get rid of the local minimum is to change the initial guess for the optimization process a couple of times to ensure that all the results are converged to a unique solution. Besides, other optimization criteria are also important; for instance, how far the algorithm can get from the initial guess when it is searching for the optimal parameters.

5.7.3 Polytropic Index and Specific Heat Ratio

Regarding the cylinder wall temperature, the first method discussed in section 3.3 is also investigated in this master thesis and figure 5.6 illustrates the polytropic index and specific heat ratio obtained for the test 2 and 6. Figure 5.7 displays the same results obtained for tests 6 and 9.

This approach is not used in this master thesis since it gives unreasonable cylinder wall temperatures in some of the studied tests. If the intersection between two curves occurs early, the cylinder wall temperature gets lower than the coolant temperature which is not physically possible; conversely, if the intersection happens too late during the compression, the cylinder wall temperature becomes unreasonably high. Due to these effects, the second method for the cylinder wall temperature, explained in section 3.3, was found more reliable in this study and was selected to continue with.

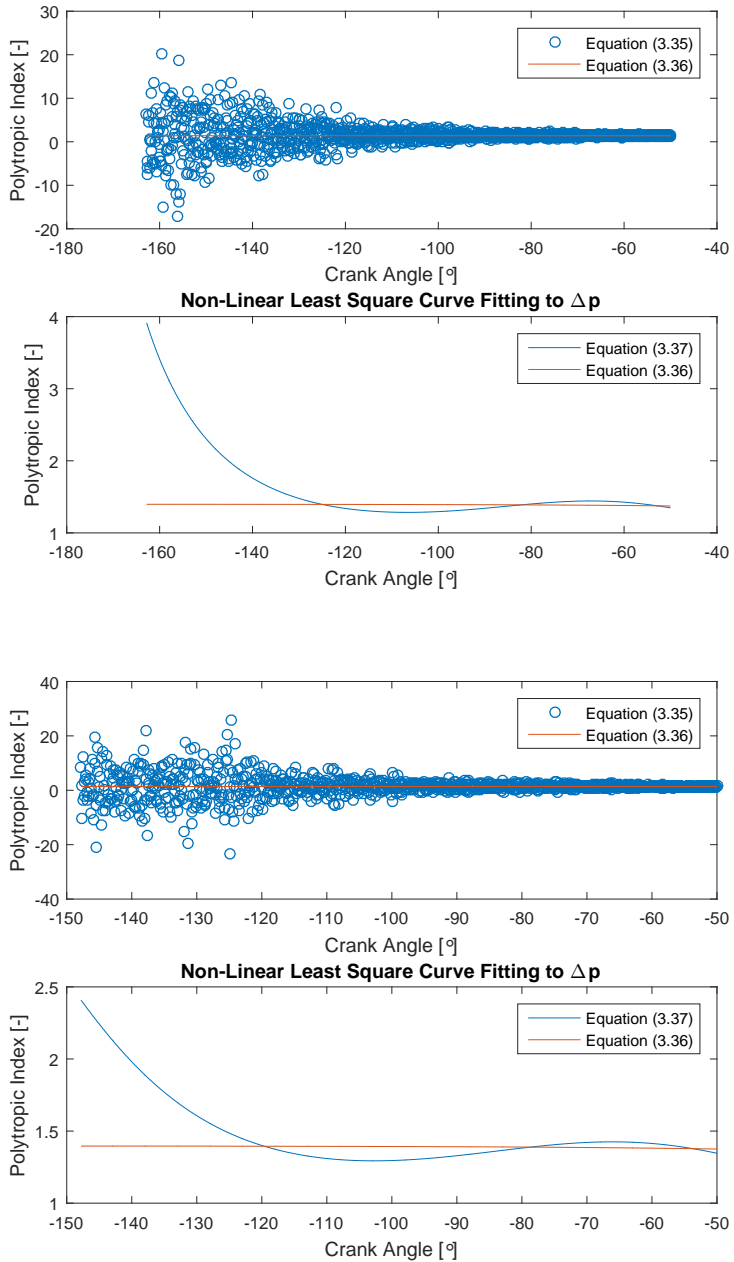


Figure 5.6: Polytropic Index and specific heat ratio for Tests 2 and 6

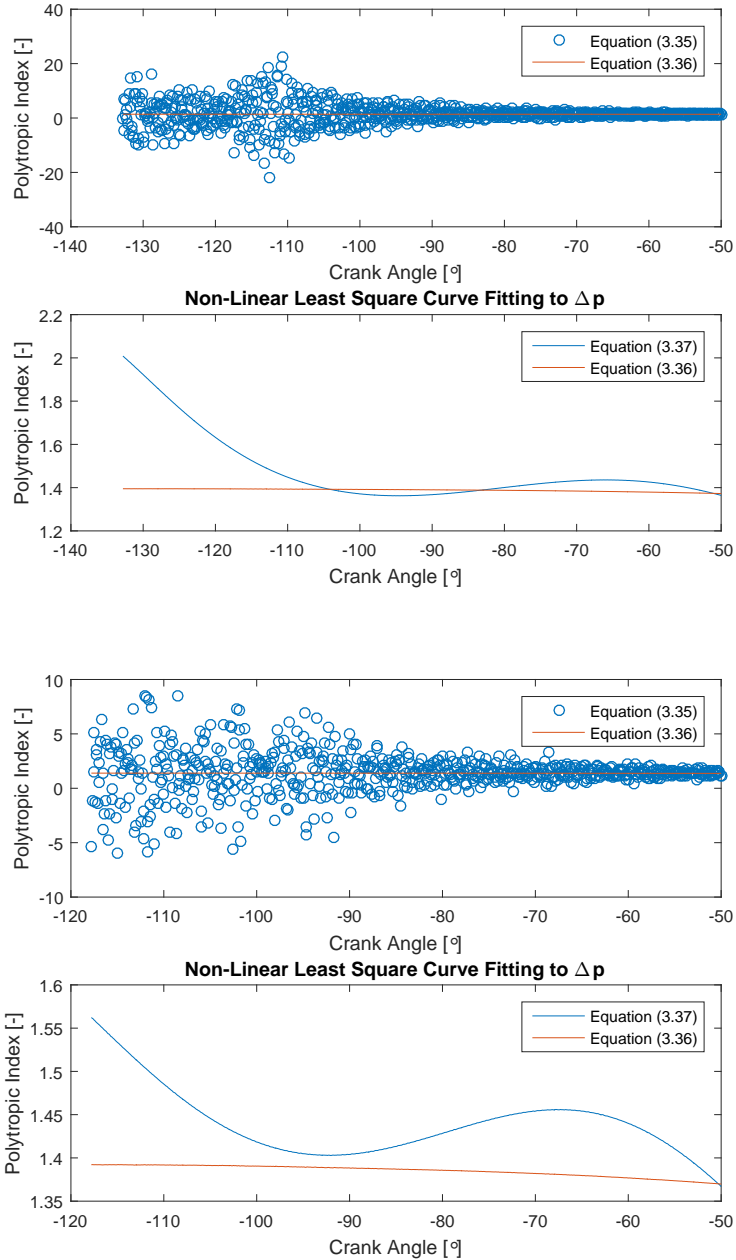


Figure 5.7: Polytropic Index and specific heat ratio for Tests 9 and 12

5.7.4 Temperature at 70° BTDC

Finally, the methodology for predicting the temperature at point *a*, 70° BTDC, is explained in section 4.11 and the results for different tests are listed in the following table,

Table 5.9: *Temperature at Point A, 70° BTDC*

Test Number	Method 1	Method 2	Method 3
	[K]	[K]	[K]
1	500.7986	496.7268	498.7627
2	505.2077	498.2758	501.7417
3	481.7764	479.9374	480.8569
4	488.3400	484.5783	486.4591
5	497.5030	491.6866	494.5948
6	483.8108	480.4472	482.1290
7	478.4555	475.0053	476.7304
8	511.0285	504.8916	507.9601
9	491.7193	486.6544	489.1869
10	495.9482	493.1177	494.5330
11	533.5103	524.4703	528.9904
12	489.6388	487.8142	488.7265

This temperature is highly influenced by the temperature at IVC which itself is dependent on the heat transfer and conditions in intake manifold and the EVC.

6

Sensitivity Analysis

After constructing a system or a mathematical model, the model inputs should be subjected to a more detailed analysis to determine how uncertainty in the model output can be addressed to the presence of uncertainty in the model inputs [14]. For this purpose, sensitivity analysis is studied. This analysis is generally a technique to evaluate how robust the model is with respect to the change in any input parameters and to examine the extent to which an independent variable can affect a dependent variable. The independent variables can be all or the most interesting inputs and the dependent variable is typically the outcome of the model [22].

There are two different approaches for conducting a sensitivity analysis, one is called the local sensitivity analysis, which is also referred to as the derivative based method where the partial derivative of the corresponding functions are studied. This approach is feasible when the correlation between inputs and output is relatively simple, however, it lacks functionality when the model is complex or when some discontinuities exist in the model [22]. Local sensitivity analysis is also known as one-at-a-time technique where only one parameter is changed and the rest of parameters are fixed and the effect of this change at a time is studied. The second approach is the global sensitivity analysis, usually using Monte Carlo techniques [22].

The aim in this chapter is to assess how the estimated air mass varies with the change in intake and exhaust valve closing temperature, cylinder wall temperature, valve lash and pressure pegging.

6.1 Intake and Exhaust Valve Closing Temperature

There exist two approaches for computing the sensitivity of the air gas mass with respect to the intake or exhaust valve closing temperatures. The first approach is

based on the balance of energy at intake valve closing and the second approach considers the air mass as the difference between the total and residual gas masses and replaces each term from ideal gas law. Note that the first approach is elaborately discussed in this chapter while the second alternative is presented in Appendix A.

The balance of energy at intake valve closing, shown by equation (4.22), is re-written as below,

$$m_{IVC}c_{v,IVC}T_{IVC} = m_{air}c_{v,air}T_{air} + m_{EVC}c_{v,res}T_{res} \quad (6.1)$$

Substituting the residual gas mass from the ideal gas law at EVC and re-arrangement of this equation gives,

$$m_{air} = \frac{m_{IVC}c_{v,IVC}T_{IVC}}{c_{v,air}T_{air}} - \frac{c_{v,res}T_{res}p_{EVC}V_{EVC}}{R_{EVC}T_{EVC}T_{air}c_{v,air}} \quad (6.2)$$

According to this equation, the second term on the right-hand-side is independent of the temperature at IVC and the only dependency of air mass on the intake valve closing temperature is captured by the first term in that equation. Therefore, taking the derivative of air mass with respect to the intake valve closing gives,

$$\frac{dm_{air}}{dT_{IVC}} = \frac{m_{IVC}c_{v,IVC}}{c_{v,air}T_{air}} \quad (6.3)$$

Equation (6.3) indicates the sensitivity of air mass to the intake valve closing temperature. Additionally, to obtain the sensitivity of air mass to the exhaust valve closing temperature, equation (6.2) can be studied once again. The first term on the right-hand-side of this equation is independent of the temperature at EVC. Therefore, any change in the exhaust valve closing temperature creates uncertainty in the air mass estimation according to the following equation,

$$\frac{dm_{air}}{dT_{EVC}} = \frac{c_{v,res}T_{res}p_{EVC}V_{EVC}}{R_{EVC}T_{EVC}^2T_{air}c_{v,air}} \quad (6.4)$$

Equation (6.4) predicts the sensitivity of the air mass to the temperature at exhaust valve closing. The last two aforementioned equations are evaluated for different tests and the results are shown in the following table.

Table 6.1: Sensitivity of Air Mass to T_{IVC} and T_{EVC}

Test Number	$\frac{dm_{air}}{dT_{IVC}}$	$\frac{dm_{air}}{dT_{EVC}}$
	[gr/K]	[gr/K]
1	20.8141	0.3498
2	19.1178	0.3323
3	9.0693	0.2741
4	11.6319	0.2642
5	14.5282	0.2882
6	8.1582	0.4890
7	7.7687	0.5587
8	10.0884	0.7098
9	6.4955	0.7525
10	6.8236	0.6433
11	5.9998	0.5644
12	5.5611	0.8529

According to the results obtained from the sensitivity analysis, despite the tests 11 and 12 with the lowest sensitivity, tests 1, 2, 4, 5 and 8 are the most sensitive tests regarding the changes the intake valve closing temperature. Besides, tests 8, 9, 10 and 12 exhibit the largest sensitivities to the changes in the exhaust valve closing temperature while the lowest sensitivities are presented in the tests 3 to 5. Moreover, it can be claimed that any uncertainty in the intake valve closing temperature has a much larger impact on the air mass estimation compared to the uncertainty in the exhaust valve closing temperature since the magnitude of partial derivatives with respect to the former is considerably larger than that of the latter. Furthermore, equation (6.3) with a negative sign implies that any over-estimation in the intake valve closing temperature results an under-estimation of the air mass and vice versa. In contrast, according to equation (??), under-estimation of exhaust valve closing temperature under-estimates the air mass and vice versa.

To study the sensitivity analysis in the rest of this chapter, the previously obtained air mass is compared to the new one according to the following equation,

$$PoC = \frac{m_{air,New} - m_{air,Old}}{m_{air,Old}} \quad (6.5)$$

where PoC is percentage of change.

6.2 Cylinder Wall Temperature

The aim in this section is to study how large the air mass estimation is affected when the cylinder wall temperature is either over- or under-estimated by 2 and 5%. The table below indicates the summary of the results obtained.

Table 6.2: Sensitivity of Air Mass to Cylinder Wall Temperature

Test Number	PoC [%]				$m_{air,Old}$ [gr]
	over-estimated		under-estimated		
	2%	5%	2%	5%	
1	-0.8341	-2.0860	0.8356	2.0875	6.8455
2	-0.8494	-2.1251	0.8510	2.1267	6.2867
3	-0.9697	-2.4278	0.9732	2.4278	2.9080
4	-0.9265	-2.3148	0.9265	2.3175	3.7670
5	-0.8903	-2.2258	0.8903	2.2279	4.7398
6	-1.1024	-2.7600	1.1064	2.7600	2.5217
7	-1.1365	-2.8413	1.1365	2.8413	2.3581
8	-1.0574	-2.6467	1.0574	2.6467	3.0453
9	-1.4998	-3.7467	1.4942	3.7411	1.7936
10	-1.4166	-3.5363	1.4166	3.5414	1.9625
11	-1.3860	-3.4622	1.3860	3.4622	1.7388
12	-1.8902	-4.7291	1.8973	4.7361	1.4231

It can be seen in this table that even 2% error in the cylinder wall temperature affects the air mass estimation by approximately 1 to 2% and the error in the air mass estimation increases by introducing larger error in cylinder wall temperature. Over-estimation of this temperature causes the under-estimation of air mass in all the tests and vice versa. This is due to the fact that the temperature at intake valve closing is calculated according to the heat transfer between the in-cylinder gas and cylinder wall temperature. Over-estimation of the temperature at cylinder wall increases the heat transfer and generates higher cylinder gas temperature at intake valve closing. Based on the ideal gas law, over-estimation of intake valve closing temperature causes under-estimation total cylinder gas mass since all the other parameters such as the pressure, volume and ideal gas constant at IVC remain unchanged. It is evident from table 6.2 that tests 1 and 2 indicate the lowest sensitivity to the changes in cylinder wall temperature while tests 9, 10, 11 and 12 are the most sensitive tests to the presence of uncertainty in the cylinder wall temperature.

6.3 Intake and Exhaust Valve Valve Lash

In general, valve lash compensates for the elongation of the valve while the engine is running. The valve lashes that are used to obtain the results indicated in the previous chapter were 1.45 and 1.7 mm for the intake and exhaust valves, respectively. Since the valve elongation is temperature-dependent and can be also affected by the temperature history, defining a constant value for each valve under all the operating conditions may not be sufficient. Due to these reasons, there is an uncertainty in the accuracy of the aforementioned values and it is essential to investigate their influence on the results. For the intake valve, 1 and 1.25 mm valve lash is studied, for the exhaust valve, however, 1.2 and 1.45, 1.6 mm are investigated. In total, the five above-mentioned cases are examined and the corresponding results are indicated in the following table,

Table 6.3: Sensitivity of Air Mass to Intake and Exhaust Valve Lash

Test Number	PoC [%]					$m_{air,Old}$ [gr]
	Case 1	Case 2	Case 3	Case 4	Case 5	
1	-0.5157	-0.2235	0.9174	0.5799	0.2556	6.8455
2	-0.4040	-0.1845	0.8892	0.5695	0.2513	6.2867
3	-0.5296	-0.2510	1.1039	0.6190	0.2613	2.9080
4	-0.4486	-0.1964	1.0194	0.6106	0.2655	3.7670
5	-0.4325	-0.1962	0.9473	0.5760	0.2553	4.7398
6	-0.3529	-0.1666	1.3602	0.7654	0.3291	2.5217
7	-0.3181	-0.1527	1.2001	0.6997	0.3053	2.3581
8	0.0525	-0.0394	0.8374	0.5287	0.2397	3.0453
9	0.0836	-0.0390	0.5520	0.4070	0.1896	1.7936
10	-0.0357	-0.0968	0.7134	0.4790	0.2191	1.9625
11	0.6614	0.1725	0.3278	0.3106	0.1610	1.7388
12	0.1897	-0.0351	0.4708	0.4005	0.1897	1.4231

It can be seen clearly that there is no specific trend in the error determined for the estimated air mass and the reason is that intake and exhaust valve lashes should not be constant over all the operating conditions. The only observation is that the high-load tests exhibit more sensitivity than the low-load tests. For instance, the variation in the air mass estimation is much less in the tests 9 and 12 compared to the tests 1, 2 and 5.

6.4 Pressure Pegging

As mentioned in chapter 4, pressure offset is the difference between the intake manifold pressure and the cylinder pressure before intake valve closes. To determine this offset, the interval for the cylinder pressure is between 170 to 165° BTDC since the latest intake valve closing happens at 163° BTDC. This pressure offset, then, is used for the pressure correction according to the following equation,

$$P_{cyl,c} = P_{cyl,m} + P_{Offset} \quad (6.6)$$

where c and m stand for corrected and measured pressures at each crank angle, respectively. In this section, the influence of either 2 or 5% deviation in the pressure offset is studied and the following table summarizes the corresponding results,

Table 6.4: Sensitivity of Air Mass to Pressure Pegging

Test Number	PoC [%]				$m_{air,Old}$ [gr]
	over-estimated		under-estimated		
	2%	5%	2%	5%	
1	-0.1841	-0.4616	0.1841	0.4616	6.8455
2	-0.1638	-0.4120	0.1654	0.4120	6.2867
3	-0.1204	-0.3026	0.1204	0.3026	2.9080
4	-0.1354	-0.3371	0.1354	0.3371	3.7670
5	-0.1498	-0.3734	0.1498	0.3734	4.7398
6	-0.1031	-0.2538	0.1031	0.2538	2.5217
7	-0.0848	-0.2163	0.0848	0.2163	2.3581
8	-0.2266	-0.5714	0.2266	0.5681	3.0453
9	0.4293	1.0816	-0.4349	-1.0928	1.7936
10	0.4127	1.0344	-0.4127	-1.0344	1.9625
11	0.4773	1.1847	-0.4773	-1.1905	1.7388
12	0.4216	1.0540	-0.4216	-1.0540	1.4231

It is evident that the pressure correction affects the air mass estimation in all the tests and the magnitude and the direction of deviation vary test to test. Tests 9, 10, 11 and 12 exhibit the highest sensitivity to pressure pegging while the lowest sensitivity can be seen in one of the tests with low engine torque, test 7. Also note that the over-estimation of the pressure offset in the tests 1 to 8 brings the under-estimation of the air mass while this trend is reversed in the tests 9 to 12.

The reason is that if the instantaneous cylinder pressure is overestimated, the increased pressure at IVC over-estimates the amount of total mass in the cylinder and the increased pressure at EVC over-estimates the residual gas mass. In the tests with small amount of residual gases, the over-estimation of total mass is more severe than that of residual gas mass; therefore, the over-estimation of cylinder pressure mainly over-estimates the amount of fresh air. However, in the tests with a larger residual gas fraction, the over-estimation of residual gases is larger than that of the total gas mass and therefore the fresh air is under-estimated.

6.5 Summary

Prediction of air mass can be influenced by the presence of uncertainty in the input parameters. In this study, the influence of uncertainty in the intake and exhaust valve closing temperatures, cylinder wall temperature, intake and exhaust valve lashes and pressure pegging is investigated and the following results are observed:

- Tests 1 and 2 demonstrate the highest sensitivity to the temperature at intake valve closing while tests 11 and 12 displays the lowest sensitivity.
- Test 12 is most sensitive to exhaust valve closing temperature; however, the lowest sensitivity can be seen in test 4.
- Tests 9 to 12 are more sensitive to cylinder wall temperature than other tests.
- Among all the studied parameters, cylinder wall temperature affect the estimation of air mass more considerably than valve lash and pressure pegging. Besides, the influence of intake valve closing temperature is larger than the exhaust valve closing temperature.

In overall, the conclusion is that the heat transfer, the temperature of the cylinder wall and the cylinder gas temperature should be determined precisely otherwise unacceptable errors in the air mass estimation may occur. Another finding is that the high-load tests require more attention to the correctness of inputs rather than the low-load tests.

7

Conclusions

A thermodynamic model is constructed for the sake of estimating the total cylinder gas mass and its composition. In overall, 60 tests are investigated, all having symmetric cam phasing with negative valve overlap.

The model is composed of two iterative sub-models, one for the residual gas mass and its temperature and the other for the total in-cylinder gas mass and the temperature at intake valve closing. The difference between these two output masses determine the amount of fresh charge entering the cylinder during the intake stroke.

Apart from the aforementioned masses and temperatures, the temperature of the residual gas mass and that of the fresh charge after heat transfer and before mixing, the gas temperature at exhaust valve opening, the compression polytropic exponent, the specific heat ratio for each point during the compression stroke, the cylinder wall temperature as well as the pressures and temperatures during the compression stroke are computed by the model. The temperature at point *a*, 70° BTDC, is calculated in three different ways.

The air mass is estimated in 5 different ways, one uses the ideal gas law at intake valve closing, the second uses the Δp method between intake valve closing and 70° BTDC, the third, fourth and fifth use the Δp method from 70° to 50° BTDC by the initial temperature obtained in three different ways. The average error in the air mass estimation is less than 1% in average and lower than 2% in all of the investigated tests. The beneficial feature of using five different approaches for the air mass estimation is that the average error is lowered when the air is underestimated by one or some of the alternatives and over-estimated by others. It is also important to note that the reason for getting high error, around 2% in two of the tests, is due to the fact that the error in all the above-mentioned approaches have the same sign for these tests and could not help to lower the average error.

The compression stroke is treated as a polytropic process following the equa-

tion $pV^k = c$ with a constant polytropic index, k . This polytropic index differs with the specific heat ratio, γ . An important observation is that both the polytropic coefficient and the total mass in the cylinder are highly influenced by choice of interval for the Δp method. A broad interval should be defined such that it serves as a true representative of the entire compression stroke and its characteristics. If the final point in this interval is selected too close to the intake valve closing, the polytropic index is over-estimated and the accuracy of the Δp method decreases. Besides, the final point should not be close to the TDC otherwise it interferes with the fuel injection time and the Δp method becomes invalid.

The cylinder wall temperature is constant in each operating cycle and is dependent on the engine speed and engine torque. The only validation used in this master thesis is that the estimated temperature for the cylinder wall should be higher than the coolant temperature. This temperature serves as the input to the spatially averaged Woschni heat transfer model to predict the cylinder gas temperature when intake valve closes.

In overall, it can be concluded that the Δp method can predict the total gas mass in the cylinder when the polytropic index and the initial temperature is either estimated or measure accurately otherwise unacceptable errors may occur.

8

Future Work

In real-world applications, the cylinder wall temperature is dependent on engine speed, load, coolant temperature and position of piston in the stroke [10]. This implies that a more detailed analysis of cylinder wall temperature can be performed, especially to consider its dependency on the distance from TDC. For this purpose, heat release analysis can be investigated.

Even though the measurement of cylinder wall temperature is hard to perform in practice, one of the potential future work is to perform experiments to measure either the cylinder wall temperature or any other temperature in the cylinder such that it can be used for better estimation of the temperature at intake valve closing.

Additionally, a more detailed heat transfer model can be implemented. The heat transfer for the residual gas can be divided into two parts, one from EVC to IVO and another from IVO to IVC. This is due to the fact that although the residual gas only transfers the heat to/from the cylinder wall between EVC and IVO, the heat transfer might occur between the residual gas, fresh charge, intake port and cylinder wall temperature depending on the operating conditions. This phenomenon is more pronounced when the intake valve opening pressure is higher than the intake manifold pressure which causes the residual gases traveling into the intake manifold and the heat is partially transferred between the residual gas mass, fresh charge, the intake manifold and cylinder wall. However, the current heat transfer model only captures the heat transfer between the cylinder gas and the cylinder wall. This effect could be considered in this master thesis but is addressed as the future work.

Pegging of the pressure trace can be performed in a better way if the intake manifold pressure is measured with respect to the crank angle, not only an average value over the whole working cycle. Besides, as mentioned previously, neither of the methods explained in chapter 4 is suitable for all the operating con-

ditions; therefore, other pressure pegging methods can be implemented with the aim of finding the most reliable method according to operating conditions. Furthermore, the mean pressure for the intake and exhaust manifold is measured in the test cells. However, comparing these mean values with the cylinder pressure cannot give any information about the direction of the flow. If the direction of the flow is unknown, the heat transfer cannot be correctly modeled and the gas properties can be only approximated. Due to this reason, recording the intake and exhaust manifold pressures based on the crack angles can have a both-edge benefit.

The influence of pressure signal resolution in the accuracy and computational expenses could not be investigated in this study since the resolution is the same in all the cases, however, another recommendation is to investigate this parameter and its effect(s).

Last but not least, only cycles with negative valve overlap are investigated. Therefore, one potential future work can be to generalize the constructed method and test it over cycles with positive valve overlap as well.

A

Another Alternative for Sensitivity of Air Mass to Intake and Exhaust Valve Closing Temperatures

The second alternative to investigate the sensitivity of air mass to the intake or exhaust valve closing temperature is to consider the air mass as the difference between the total and residual gas masses, as indicated by the following equation,

$$m_{air} = m_{IVC} - m_{EVC} \quad (A.1)$$

Substituting the total and the residual gas masses from the ideal gas law, the following equation yields,

$$m_{air} = \frac{p_{IVC}V_{IVC}}{R_{IVC}T_{IVC}} - \frac{p_{EVC}V_{EVC}}{R_{EVC}T_{EVC}} \quad (A.2)$$

This equation displays the correlation between air mass and conditions at intake and exhaust valve closing. According to this equation and the method explained in sections 4.7 and 4.9, the temperature at exhaust valve closing is independent of that at intake valve closing while the latter is dependent on the former. Hence, taking the partial derivative of equation (A.2) with respect to the temperature at intake valve closing gives,

$$\frac{dm_{air}}{dT_{IVC}} = -\frac{p_{IVC}V_{IVC}}{R_{IVC}T_{IVC}^2} \quad (A.3)$$

Similarly, taking the partial derivative of equation (A.2) with respect to the temperature at exhaust valve closing yields,

$$\frac{dm_{air}}{dT_{EVC}} = -\frac{p_{IVC}V_{IVC}}{R_{IVC}T_{IVC}^2} \frac{dT_{IVC}}{dT_{EVC}} + \frac{p_{EVC}V_{EVC}}{R_{EVC}T_{EVC}^2} \quad (A.4)$$

Since determination of $\frac{dT_{IVC}}{dT_{EVC}}$ is complex, this approach is not preferred in this study.

B

A Complete Set of Results

Table B.1: Test 1 - IVO: -354.7; IVC: -162.8; EVO: 144.3; EVC: 350.2

		cycle 1	cycle 2	cycle 3	cycle 4	cycle 5
Engine Speed [rpm]		1200.0430	1200.0800	1200.0250	1200.0830	1200.0370
Engine Torque [Nm]		2464.1250	2463.9370	2463.8950	2463.8070	2463.7920
p_{im} [kPa]		316.2375	302.1966	296.6870	294.3750	292.0920
p_{em} [kPa]		276.8005	262.2294	255.9313	253.1178	251.0132
T_{im} [K]		304.9772	304.5614	304.3694	304.2729	304.1531
T_{em} [K]		773.9854	760.4777	755.2296	749.7286	749.2675
T_{cb} [K]		359.1381	359.5434	357.7729	357.4490	357.1841
T_{ca} [K]		362.8984	363.6284	362.9154	362.7898	362.7877
\dot{m}_{air} [gr/s]		69.9115	66.4213	65.0007	64.4239	63.8431
m_{air} [gr]		6.9909	6.6417	6.4999	6.4419	6.3841
λ [-]		1.8252	1.7817	1.7587	1.7458	1.7293
p_{IVO} [kPa]		266.5343	253.1928	249.0661	245.8404	242.0787
p_{IVC} [kPa]		315.5803	302.3650	297.2648	295.8381	293.7242
p_{EVO} [kPa]		1084.8910	1016.0316	988.2028	971.9873	965.3073
p_{EVC} [kPa]		240.0704	229.4942	223.3691	220.5066	216.8133
m_{EVC} [gr]		0.1308	0.1269	0.1245	0.1239	0.1221
$x_{b,res}$ [%]		56.4336	57.7599	58.4863	58.9026	59.4444
$x_{b,IVC}$ [%]		1.0527	1.0924	1.1036	1.1118	1.1141
T_{EVC} [K]		746.9085	735.4914	729.8958	724.2180	722.2223
T_{fc} [K]		335.6770	335.8883	335.9716	336.1691	336.1709
T_{res} [K]		612.3710	608.6445	607.2524	607.1115	606.1240
T_{IVC} [K]		341.6843	341.8843	341.9168	342.1010	342.0395
T_a [K]		500.7986	501.2125	503.0957	502.9634	503.3829
		496.7268	496.5861	497.6182	497.2772	497.6811
		498.7627	498.8993	500.3569	500.1203	500.5320
T_w [K]		407.8131	407.8118	407.8103	407.8104	407.8094
k	IVC: 70°	1.4559	1.4562	1.4606	1.4596	1.4608
	70 : 50°	1.4029	1.4012	1.3992	1.3983	1.3990
m_{IVC} [gr]	IGL	7.0096	6.7121	6.5983	6.5631	6.5174
	IVC: 70°	6.9287	6.6243	6.4966	6.4580	6.4128
	70: 50°	6.9526	6.6502	6.5264	6.4889	6.4435
	70: 50°	7.0096	6.7121	6.5983	6.5631	6.5174
	70: 50°	6.9810	6.6810	6.5622	6.5258	6.4802
Average	6.9763	6.6759	6.5563	6.5198	6.4743	
m_{air} [gr]	IGL	6.8788	6.5852	6.4738	6.4392	6.3952
	IVC: 70°	6.7980	6.4973	6.3720	6.3341	6.2907
	70: 50°	6.8218	6.5232	6.4019	6.3650	6.3214
	70: 50°	6.8788	6.5852	6.4738	6.4392	6.3952
	70: 50°	6.8502	6.5541	6.4377	6.4019	6.3581
Average	6.8455	6.5490	6.4318	6.3959	6.3521	
$m_{air,err}$ [%]	IGL	-1.6033	-0.8508	-0.4025	-0.0426	0.1738
	IVC: 70°	-2.7596	-2.1737	-1.9676	-1.6741	-1.4635
	70: 50°	-2.4186	-1.7836	-1.5078	-1.1944	-0.9825
	70: 50°	-1.6033	-0.8508	-0.4025	-0.0426	0.1738
	70: 50°	-2.0126	-1.3194	-0.9582	-0.6217	-0.4076
Average	-2.0795	-1.3957	-1.0477	-0.7151	-0.5012	

Table B.2: Test 2- IVO:-354.7 ; IVC: -162.8; EVO: 144.3; EVC: 350.2

		cycle 1	cycle 2	cycle 3	cycle 4	cycle 5	cycle 6	cycle 7
Engine Speed		1200.0670	1200.0460	1200.0710	1200.0510	1200.0660	1200.0660	1200.0670
Engine Torque		2464.1320	2463.6920	2464.0430	2463.9360	2464.0210	2464.4390	2464.2470
P_{im}		289.5136	290.7332	293.9428	300.8427	314.8937	328.1746	327.2950
P_{em}		249.9209	250.9430	253.6752	260.3496	275.1086	289.9182	281.4416
T_{im}		303.5989	303.9951	304.1630	304.4837	305.2500	306.1549	306.4843
T_{em}		742.1706	751.0154	748.1914	754.8611	765.3421	784.3543	814.6988
T_{cb}		358.2601	357.8001	357.4515	357.2781	357.2558	356.9421	356.7650
T_{ca}		362.8175	362.9620	362.8327	362.7929	362.7625	362.7281	362.7647
\dot{m}_{air}		63.0970	63.3694	64.1723	65.8719	69.2524	72.2465	72.2381
m_{air}		6.3094	6.3367	6.4169	6.5869	6.9249	7.2242	7.2234
λ		1.7066	1.7119	1.7307	1.7620	1.8067	1.8258	1.7768
P_{IVO}		242.1418	243.1617	245.8178	252.1411	261.9033	270.4996	264.4800
P_{IVC}		290.6017	291.7149	294.8491	301.8441	316.3561	329.7641	327.8975
P_{EVO}		954.3026	965.2872	981.1822	1015.0866	1082.2529	1153.5204	1196.3284
P_{EVC}		212.3063	213.9486	217.8206	224.0131	237.2347	248.1944	237.2828
m_{EVC}		0.1213	0.1206	0.1231	0.1254	0.1309	0.1338	0.1236
$x_{b,res}$		60.2044	60.0236	59.3961	58.3820	56.9897	56.4154	57.9153
$x_{b,IVC}$		1.1302	1.1177	1.1165	1.0925	1.0635	1.0343	0.9861
T_{EVC}		712.3463	721.5552	720.0994	726.9170	737.4554	754.5078	780.9730
T_{fc}		335.7020	335.9244	335.9560	336.0413	336.3747	336.7594	336.7422
T_{res}		598.4931	603.7256	602.8052	606.7469	612.7173	623.9050	639.6688
T_{IVC}		341.4235	341.7144	341.7761	341.9196	342.3626	342.8857	342.7721
T_a		505.2077	505.1892	504.5028	503.8832	503.4337	503.7862	503.9253
		498.2758	498.5734	498.0842	497.8496	497.2871	497.7714	498.3985
		501.7417	501.8813	501.2935	500.8664	500.3604	500.7788	501.1619
T_w		407.8136	407.8085	407.8127	407.8112	407.8124	407.8169	407.8149
k	IVC: 70°	1.4673	1.4662	1.4644	1.4624	1.4598	1.4588	1.4595
	70 : 50°	1.3951	1.3968	1.3978	1.3976	1.3963	1.3969	1.3992
m_{IVC}	IGL	6.4597	6.4789	6.5474	6.6999	7.0129	7.2989	7.2600
	IVC: 70°	6.3345	6.3590	6.4296	6.5863	6.8916	7.1755	7.1472
	70: 50°	6.3711	6.3941	6.4641	6.6196	6.9273	7.2118	7.1804
	70: 50°	6.4597	6.4789	6.5474	6.6999	7.0129	7.2989	7.2600
	70: 50°	6.4151	6.4362	6.5054	6.6595	6.9698	7.2551	7.2200
	Average	6.4080	6.4294	6.4988	6.6530	6.9629	7.2481	7.2135
m_{air}	IGL	6.3384	6.3583	6.4243	6.5745	6.8820	7.1651	7.1364
	IVC: 70°	6.2132	6.2384	6.3065	6.4610	6.7607	7.0416	7.0236
	70: 50°	6.2498	6.2734	6.3410	6.4943	6.7964	7.0780	7.0568
	70: 50°	6.3384	6.3583	6.4243	6.5745	6.8820	7.1651	7.1364
	70: 50°	6.2938	6.3156	6.3824	6.5341	6.8389	7.1213	7.0964
	Average	6.2867	6.3088	6.3757	6.5277	6.8320	7.1142	7.0899
$m_{air,err}$	IGL	0.4611	0.3406	0.1158	-0.1885	-0.6187	-0.8184	-1.2044
	IVC: 70°	-1.5236	-1.5517	-1.7200	-1.9121	-2.3700	-2.5276	-2.7659
	70: 50°	-0.9437	-0.9983	-1.1823	-1.4065	-1.8551	-2.0247	-2.3067
	70: 50°	0.4611	0.3406	0.1158	-0.1885	-0.6187	-0.8184	-1.2044
	70: 50°	-0.2462	-0.3333	-0.5374	-0.8012	-1.2407	-1.4252	-1.7586
	Average	-0.3583	-0.4404	-0.6416	-0.8994	-1.3407	-1.5229	-1.8480

Table B.3: Test 3- IVO:-354.7; IVC:-162.8; EVO:144.3; EVC:350.2

		cycle 1	cycle 2	cycle 3	cycle 4	cycle 5
Engine Speed		1200.0510	1200.0720	1200.0420	1200.0820	1200.0480
Engine Torque		560.5019	560.3979	560.1041	560.5572	560.4445
p_{im}		134.1495	134.9760	136.5954	140.0419	144.4816
p_{em}		134.8955	135.2786	136.2564	138.4625	141.1606
T_{im}		301.7718	301.7558	301.5937	301.5874	301.4804
T_{em}		541.3159	547.8026	555.5975	568.0564	579.9510
T_{cb}		361.4592	361.8422	361.5761	361.3829	361.5177
T_{ca}		362.9136	362.9909	363.1616	362.9762	362.8947
m_{air}		29.0382	29.2761	29.7262	30.5678	31.6025
m_{air}		2.9037	2.9274	2.9725	3.0566	3.1601
λ		2.9581	2.9787	2.9984	3.0055	2.9885
p_{IVO}		130.7678	131.9655	132.8135	134.4276	138.4497
p_{IVC}		134.1567	134.7770	136.5195	140.2121	144.4090
p_{EVO}		303.5499	310.1926	321.7528	340.5916	361.9808
p_{EVC}		138.4930	139.0207	138.9876	139.4593	141.1751
m_{EVC}		0.1032	0.1024	0.1011	0.0996	0.0989
$x_{b,res}$		35.3134	35.0742	34.8493	34.7685	34.9616
$x_{b,IVC}$		1.2077	1.1836	1.1464	1.0964	1.0621
T_{EVC}		545.1425	551.8126	558.5487	569.1426	579.9669
T_{fc}		332.5110	332.3401	332.1941	332.1044	331.6685
T_{res}		462.0917	464.7117	469.4056	475.8228	481.3155
T_{IVC}		337.3700	337.2428	337.1473	337.0821	336.6716
T_a		481.7764	481.4005	480.0811	480.9188	481.3582
		479.9374	479.5046	478.3731	478.4762	479.3419
		480.8569	480.4525	479.2271	479.6975	480.3500
T_w		387.3356	387.3348	387.3311	387.3367	387.3349
k	IVC: 70°	1.4249	1.4244	1.4215	1.4238	1.4263
	70 : 50°	1.3937	1.3940	1.3940	1.3913	1.3909
m_{IVC}	IGL	3.0180	3.0331	3.0732	3.1569	3.2553
	IVC: 70°	3.0015	3.0159	3.0575	3.1339	3.2358
	70: 50°	3.0065	3.0211	3.0622	3.1408	3.2417
	70: 50°	3.0180	3.0331	3.0732	3.1569	3.2553
	70: 50°	3.0122	3.0271	3.0677	3.1488	3.2485
	Average	3.0112	3.0261	3.0667	3.1475	3.2473
m_{air}	IGL	2.9148	2.9307	2.9721	3.0573	3.1564
	IVC: 70°	2.8982	2.9136	2.9564	3.0343	3.1369
	70: 50°	2.9032	2.9188	2.9611	3.0413	3.1428
	70: 50°	2.9148	2.9307	2.9721	3.0573	3.1564
	70: 50°	2.9090	2.9247	2.9666	3.0493	3.1496
	Average	2.9080	2.9237	2.9656	3.0479	3.1484
$m_{air,err}$	IGL	0.3810	0.1122	-0.0157	0.0247	-0.1168
	IVC: 70°	-0.1880	-0.4731	-0.5438	-0.7279	-0.7353
	70: 50°	-0.0158	-0.2958	-0.3835	-0.4999	-0.5483
	70: 50°	0.3810	0.1122	-0.0157	0.0247	-0.1168
	70: 50°	0.1822	-0.0922	-0.1999	-0.2383	-0.3330
	Average	0.1481	-0.1274	-0.2317	-0.2833	-0.3700

Table B.4: Test 4- IVO:-354.7; IVC:-162.8; EVO:144.3; EVC:350.2

		cycle 1	cycle 2	cycle 3	cycle 4	cycle 5
Engine Speed		1200.0570	1200.0900	1200.0460	1200.0710	1200.0550
Engine Torque		1163.7790	1163.5060	1163.5780	1163.5460	1163.3140
p_{im}		172.5897	176.7105	182.9799	192.0776	201.5228
p_{em}		158.2876	161.4453	166.0960	172.8349	180.0490
T_{im}		301.3046	301.5106	301.5012	301.5262	301.4883
T_{em}		630.0424	631.6283	639.6046	653.8104	660.6050
T_{cb}		360.3832	360.1918	360.1242	360.1272	359.9073
T_{ca}		362.9158	362.8928	362.8732	362.9353	362.8201
\dot{m}_{air}		37.4630	38.5170	40.0864	42.2097	44.3497
m_{air}		3.7461	3.8514	4.0085	4.2207	4.4348
λ		2.0729	2.1303	2.1820	2.2253	2.2574
p_{IVO}		483.2966	501.3492	525.8167	568.9159	611.7657
p_{IVC}		152.7873	155.0538	159.8581	164.7187	171.9407
p_{EVO}		159.4059	163.7215	167.8322	174.3109	182.3195
p_{EVC}		173.1265	177.3545	184.1751	193.6999	203.3159
m_{EVC}		0.0995	0.1009	0.1026	0.1037	0.1071
$x_{b,res}$		49.9064	48.6041	47.4885	46.5920	45.9496
$x_{b,IVC}$		1.2788	1.2321	1.1794	1.1113	1.0774
T_{EVC}		624.2883	625.0380	633.2855	645.7230	652.7836
T_{fc}		332.9370	332.9367	332.8788	332.6756	332.3554
T_{res}		517.9868	519.7874	524.3967	534.6581	540.8082
T_{IVC}		338.2888	338.2721	338.2359	338.0999	337.8591
T_a		488.3400	487.0525	487.7077	486.9532	487.0965
		484.5783	483.7547	483.3289	482.6092	482.8589
		486.4591	485.4036	485.5183	484.7812	484.9777
T_w		393.8253	393.8229	393.8229	393.8230	393.8202
k	IVC: 70°	1.4378	1.4347	1.4364	1.4350	1.4362
	70 : 50°	1.3920	1.3922	1.3902	1.3885	1.3875
m_{IVC}	IGL	3.8841	3.9791	4.1326	4.3480	4.5671
	IVC: 70°	3.8414	3.9406	4.0796	4.2926	4.5104
	70: 50°	3.8542	3.9522	4.0955	4.3092	4.5274
	70: 50°	3.8841	3.9791	4.1326	4.3480	4.5671
	70: 50°	3.8691	3.9656	4.1139	4.3285	4.5472
Average	3.8666	3.9633	4.1108	4.3253	4.5438	
m_{air}	IGL	3.7846	3.8783	4.0299	4.2443	4.4600
	IVC: 70°	3.7418	3.8397	3.9770	4.1889	4.4033
	70: 50°	3.7546	3.8513	3.9928	4.2055	4.4203
	70: 50°	3.7846	3.8783	4.0299	4.2443	4.4600
	70: 50°	3.7695	3.8647	4.0113	4.2248	4.4401
Average	3.7670	3.8625	4.0082	4.2216	4.4368	
$m_{air,err}$	IGL	1.0259	0.6968	0.5353	0.5591	0.5699
	IVC: 70°	-0.1142	-0.3029	-0.7867	-0.7540	-0.7098
	70: 50°	0.2273	-0.0027	-0.3904	-0.3598	-0.3261
	70: 50°	1.0259	0.6968	0.5353	0.5591	0.5699
	70: 50°	0.6251	0.3459	0.0703	0.0976	0.1199
Average	0.5580	0.2868	-0.0073	0.0204	0.0448	

Table B.5: Test 5- IVO:-354.7; IVC:-162.8; EVO:144.3; EVC:350.2

	cycle 1	cycle 2	cycle 3	cycle 4	cycle 5	cycle 6	cycle 7	cycle 8	
Engine Speed	1200.0490	1200.0720	1200.0400	1200.0710	1200.0420	1200.0720	1200.0410	1200.0820	
Engine Torque	1753.8040	1753.8520	1753.5410	1753.6000	1753.3530	1753.6520	1753.6670	1753.7130	
p_{im}	217.2658	218.2299	219.7274	221.5377	228.4552	238.6660	250.5687	270.6792	
p_{em}	189.9173	190.7614	192.0033	193.4698	199.4925	207.7727	217.4714	235.1859	
T_{im}	301.9391	301.9054	301.9384	301.9625	302.1050	302.2815	302.5947	303.0773	
T_{em}	675.5197	676.8078	677.2238	675.5741	683.5737	694.8635	703.7988	714.4278	
T_{cb}	358.6386	358.5363	358.6365	358.4174	358.5831	358.5487	358.5683	358.4999	
T_{ca}	362.8508	362.8094	362.8777	362.8078	362.7711	362.7958	362.7436	362.7988	
m_{air}	46.9722	47.1763	47.5270	47.9675	49.7453	52.3136	55.1771	60.1809	
m_{air}	4.6970	4.7174	4.7525	4.7965	4.9744	5.2310	5.5175	6.0177	
λ	1.7882	1.7960	1.8086	1.8221	1.8780	1.9362	1.9867	2.0494	
p_{IVO}	189.8300	191.5051	193.4378	195.3431	200.2525	209.7770	217.7039	232.0797	
p_{IVC}	218.2347	219.0311	221.0251	222.7307	229.5663	239.7499	251.2991	271.9487	
p_{EVO}	650.4872	657.7852	672.1382	679.8445	713.2958	762.1455	815.6257	911.7481	
p_{EVC}	170.4631	172.3272	172.5605	173.5603	179.5489	188.3625	195.5938	211.5370	
m_{EVC}	0.1055	0.1063	0.1065	0.1075	0.1098	0.1131	0.1161	0.1237	
$x_{b,res}$	57.5573	57.3183	56.9339	56.5267	54.9033	53.3090	52.0014	50.4622	
$x_{b,IVC}$	1.2451	1.2442	1.2276	1.2198	1.1737	1.1235	1.0734	1.0255	
T_{EVC}	657.1161	659.4606	658.9924	657.0640	665.4127	677.6864	685.0221	695.3996	
T_{fc}	334.0411	333.9378	334.0593	333.9857	333.8297	333.6273	333.3883	333.3378	
T_{res}	554.5759	554.6140	555.5525	556.5047	559.8908	565.8972	571.7303	579.7465	
T_{IVC}	339.4958	339.4182	339.5175	339.4668	339.3455	339.2180	339.0037	339.0548	
T_a	497.5030	497.8235	496.9724	496.2080	494.9787	495.0611	495.0011	495.1330	
	491.6866	491.9120	491.0148	490.6463	489.6322	489.5974	489.6982	489.7121	
	494.5948	494.8677	493.9936	493.4272	492.3055	492.3293	492.3497	492.4225	
T_w	400.1721	400.1731	400.1692	400.1704	400.1672	400.1709	400.1705	400.1718	
k	IVC: 70°	1.4557	1.4567	1.4543	1.4527	1.4502	1.4508	1.4514	1.4515
	70 : 50°	1.3929	1.3942	1.3925	1.3941	1.3932	1.3931	1.3943	1.3942
m_{IVC}	IGL	4.8787	4.8976	4.9407	4.9796	5.1342	5.3640	5.6259	6.0873
	IVC: 70°	4.7978	4.8151	4.8567	4.9003	5.0554	5.2799	5.5403	5.9926
	70: 50°	4.8216	4.8394	4.8815	4.9238	5.0788	5.3048	5.5656	6.0206
	70: 50°	4.8787	4.8976	4.9407	4.9796	5.1342	5.3640	5.6259	6.0873
	70: 50°	4.8500	4.8683	4.9109	4.9515	5.1064	5.3342	5.5956	6.0538
	Average	4.8453	4.8636	4.9061	4.9470	5.1018	5.3294	5.5907	6.0483
m_{air}	IGL	4.7731	4.7913	4.8342	4.8721	5.0245	5.2509	5.5098	5.9636
	IVC: 70°	4.6922	4.7088	4.7501	4.7929	4.9457	5.1668	5.4242	5.8689
	70: 50°	4.7161	4.7331	4.7750	4.8163	4.9690	5.1917	5.4495	5.8969
	70: 50°	4.7731	4.7913	4.8342	4.8721	5.0245	5.2509	5.5098	5.9636
	70: 50°	4.7444	4.7620	4.8044	4.8441	4.9966	5.2212	5.4795	5.9301
	Average	4.7398	4.7573	4.7996	4.8395	4.9920	5.2163	5.4746	5.9246
$m_{air,err}$	IGL	1.6201	1.5671	1.7180	1.5777	1.0075	0.3803	-0.1401	-0.8991
	IVC: 70°	-0.1023	-0.1810	-0.0506	-0.0746	-0.5770	-1.2277	-1.6918	-2.4724
	70: 50°	0.4058	0.3343	0.4717	0.4140	-0.1074	-0.7513	-1.2324	-2.0066
	70: 50°	1.6202	1.5671	1.7180	1.5777	1.0075	0.3803	-0.1400	-0.8991
	70: 50°	1.0094	0.9470	1.0911	0.9926	0.4470	-0.1886	-0.6892	-1.4559
	Average	0.9106	0.8469	0.9896	0.8975	0.3555	-0.2814	-0.7787	-1.5466

Table B.6: Test 6- IVO:-339.7; IVC:-147.8; EVO:129.3; EVC:335.2

		cycle 1	cycle 2	cycle 3	cycle 4
Engine Speed		1200.0730	1200.0430	1200.0780	1200.0460
Engine Torque		362.1437	362.5910	362.5566	362.3676
p_{im}		127.7021	128.6597	130.1865	132.4247
p_{em}		125.4718	126.1661	127.2053	128.6605
T_{im}		305.3910	305.6106	305.5962	305.3603
T_{em}		515.3054	520.7572	527.5832	535.9599
T_{cb}		361.9838	363.0971	361.7888	361.7193
T_{ca}		363.1999	364.2220	363.1185	363.0416
\dot{m}_{air}		25.0644	25.2924	25.6922	26.2423
m_{air}		2.5063	2.5291	2.5691	2.6241
λ		3.5082	3.5252	3.5349	3.5348
p_{IVO}		136.1273	134.9901	134.4626	132.9110
p_{IVC}		130.6067	131.8522	133.3117	135.9648
p_{EVO}		272.6716	278.3634	289.6440	305.7341
p_{EVC}		170.3414	169.7226	169.0235	169.3038
m_{EVC}		0.2370	0.2343	0.2311	0.2284
$x_{b,res}$		29.8821	29.7411	29.6612	29.6615
$x_{b,IVC}$		2.5566	2.4939	2.4266	2.3542
T_{EVC}		559.3024	563.7936	569.2499	576.7145
T_{fc}		339.0534	339.2338	339.0347	338.9093
T_{res}		382.5852	385.7474	389.7258	395.9024
T_{IVC}		344.3094	344.6599	344.7050	344.9641
T_a		483.8108	484.1935	484.6210	485.3584
		480.4472	480.4809	480.7751	481.1662
		482.1290	482.3372	482.6981	483.2623
T_w		385.2022	385.2065	385.2067	385.2041
k	IVC: 70°	1.4252	1.4249	1.4258	1.4268
	70 : 50°	1.3901	1.3882	1.3884	1.3845
m_{IVC}	IGL	2.7702	2.7937	2.8243	2.8783
	IVC: 70°	2.7702	2.7937	2.8243	2.8783
	70: 50°	2.7509	2.7723	2.8018	2.8534
	70: 50°	2.7702	2.7937	2.8243	2.8783
	70: 50°	2.7605	2.7830	2.8130	2.8658
	Average	2.7587	2.7810	2.8109	2.8635
m_{air}	IGL	2.5332	2.5595	2.5932	2.6498
	IVC: 70°	2.5048	2.5280	2.5603	2.6133
	70: 50°	2.5139	2.5380	2.5708	2.6250
	70: 50°	2.5332	2.5595	2.5932	2.6498
	70: 50°	2.5235	2.5487	2.5820	2.6374
	Average	2.5217	2.5467	2.5799	2.6351
$m_{air,err}$	IGL	1.0719	1.1985	0.9400	0.9800
	IVC: 70°	-0.0578	-0.0468	-0.3423	-0.4119
	70: 50°	0.3035	0.3515	0.0675	0.0326
	70: 50°	1.0719	1.1985	0.9400	0.9800
	70: 50°	0.6863	0.7734	0.5020	0.5042
	Average	0.6152	0.6950	0.4215	0.4170

Table B.7: Test 7- IVO:-339.7; IVC:-147.8; EVO:129.3; EVC:335.2

		cycle 1	cycle 2	cycle 3	cycle 4
Engine Speed		1200.0650	1200.0570	1200.0700	1200.0470
Engine Torque		162.4362	162.4348	162.5665	162.5431
P_{im}		120.4159	120.3855	120.6958	121.3804
P_{em}		121.8454	121.7963	121.8946	122.1566
T_{im}		305.6108	305.6332	305.6174	305.5504
T_{em}		457.4648	459.8478	465.4384	473.1490
T_{cb}		361.8940	361.8367	361.9629	361.8949
T_{ca}		362.8722	362.7968	362.8841	362.7856
\dot{m}_{air}		23.3166	23.3433	23.4620	23.6701
m_{air}		2.3315	2.3342	2.3461	2.3669
λ		5.1491	5.1412	5.0994	5.0376
p_{IVO}		149.0345	145.3500	145.2378	141.9127
p_{IVC}		123.5706	123.6652	123.9808	124.3303
p_{EVO}		211.4204	215.4898	221.2819	228.1290
p_{EVC}		177.5874	176.2499	174.8480	173.1416
m_{EVC}		0.2724	0.2695	0.2648	0.2588
$x_{b,res}$		20.4856	20.5165	20.6825	20.9329
$x_{b,IVC}$		2.1123	2.0925	2.0686	2.0410
T_{EVC}		507.0418	508.6693	513.5609	520.2899
T_{fc}		339.2620	339.3217	339.2444	338.9054
T_{res}		348.5100	350.1639	352.9397	356.9813
T_{IVC}		341.5751	341.7808	341.9681	342.0270
T_a		478.4555	478.7485	479.3216	478.9305
		475.0053	474.9988	475.3254	475.7574
		476.7304	476.8737	477.3235	477.3439
T_w		383.0538	383.0536	383.0552	383.0546
k	IVC: 70°	1.4212	1.4213	1.4221	1.4208
	70 : 50°	1.3877	1.3857	1.3858	1.3883
m_{IVC}	IGL	2.6418	2.6423	2.6475	2.6545
	IVC: 70°	2.6138	2.6118	2.6151	2.6287
	70: 50°	2.6228	2.6216	2.6255	2.6370
	70: 50°	2.6418	2.6423	2.6475	2.6545
	70: 50°	2.6323	2.6319	2.6365	2.6457
Average	2.6305	2.6299	2.6344	2.6441	
m_{air}	IGL	2.3694	2.3728	2.3828	2.3957
	IVC: 70°	2.3414	2.3423	2.3503	2.3698
	70: 50°	2.3504	2.3521	2.3607	2.3781
	70: 50°	2.3694	2.3728	2.3828	2.3957
	70: 50°	2.3599	2.3624	2.3717	2.3869
Average	2.3581	2.3605	2.3696	2.3853	
$m_{air,err}$	IGL	1.6254	1.6517	1.5638	1.2172
	IVC: 70°	0.4224	0.3464	0.1791	0.1231
	70: 50°	0.8083	0.7651	0.6230	0.4742
	70: 50°	1.6254	1.6517	1.5638	1.2172
	70: 50°	1.2154	1.2066	1.0914	0.8445
Average	1.1394	1.1243	1.0042	0.7752	

Table B.8: Test 8- IVO:-339.7; IVC:-147.8; EVO:129.3; EVC:335.2

		cycle 1	cycle 2	cycle 3	cycle 4
Engine Speed		1800.0200	1800.0310	1799.9720	1800.0150
Engine Torque		317.3793	317.3265	317.9241	317.3287
p_{im}		160.5840	162.6273	165.9219	170.1401
p_{em}		165.1085	166.7798	169.5141	173.2620
T_{im}		305.6379	305.6821	305.7575	305.6884
T_{em}		520.1937	524.5893	530.7889	538.6452
T_{cb}		361.5416	361.3647	361.1579	360.9786
T_{ca}		362.9640	362.8950	362.8304	362.7825
\dot{m}_{air}		46.7015	47.3597	48.3703	49.8361
m_{air}		3.1134	3.1573	3.2247	3.3224
λ		3.9781	4.0150	4.0381	4.0617
p_{IVO}		271.5619	273.9802	277.2642	278.8191
p_{IVC}		163.7019	165.0938	168.7651	173.0013
p_{EVO}		319.1515	326.9761	337.3382	353.0134
p_{EVC}		289.7227	290.9007	294.3279	296.8921
m_{EVC}		0.3731	0.3721	0.3726	0.3718
$x_{b,res}$		26.4131	26.1740	26.0271	25.8780
$x_{b,IVC}$		2.8626	2.8041	2.7344	2.6460
T_{EVC}		604.1282	608.1925	614.5145	621.2997
T_{fc}		339.9255	339.5423	339.5423	339.2169
T_{res}		382.7739	385.0130	389.2776	393.4999
T_{IVC}		347.2516	347.1058	347.4771	347.4756
T_a		511.0285	510.3817	510.8272	510.8442
		504.8916	505.0601	505.2725	505.7335
		507.9601	507.7209	508.0498	508.2888
T_w		395.5823	395.5819	395.5873	395.5817
k	IVC: 70°	1.4830	1.4819	1.4817	1.4817
	70 : 50°	1.4077	1.4096	1.4077	1.4094
m_{IVC}	IGL	3.4427	3.4735	3.5469	3.6359
	IVC: 70°	3.3832	3.4213	3.4914	3.5835
	70: 50°	3.4014	3.4372	3.5083	3.5996
	70: 50°	3.4427	3.4735	3.5469	3.6359
	70: 50°	3.4219	3.4553	3.5275	3.6176
	Average	3.4184	3.4521	3.5242	3.6145
m_{air}	IGL	3.0696	3.1013	3.1743	3.2642
	IVC: 70°	3.0101	3.0492	3.1187	3.2118
	70: 50°	3.0283	3.0651	3.1357	3.2278
	70: 50°	3.0696	3.1013	3.1743	3.2642
	70: 50°	3.0488	3.0831	3.1549	3.2459
	Average	3.0453	3.0800	3.1516	3.2427
$m_{air,err}$	IGL	-1.4059	-1.7712	-1.5652	-1.7525
	IVC: 70°	-3.3175	-3.4230	-3.2877	-3.3293
	70: 50°	-2.7339	-2.9183	-2.7612	-2.8474
	70: 50°	-1.4059	-1.7712	-1.5652	-1.7525
	70: 50°	-2.0739	-2.3477	-2.1665	-2.3027
	Average	-2.1874	-2.4463	-2.2691	-2.3969

Table B.9: Test 9- IVO:-324.7; IVC:-132.8; EVO:114.3; EVC:320.2

		cycle 1	cycle 2	cycle 3	cycle 4	cycle 5
Engine Speed		1200.0570	1200.0540	1200.0380	1200.0470	1200.0470
Engine Torque		163.5386	163.3084	163.9254	163.2392	163.8316
p_{im}		115.7748	115.8142	116.1720	116.7127	117.5185
p_{em}		114.4464	114.5887	114.8445	115.1202	115.6666
T_{im}		311.3936	311.3290	311.3573	311.4756	311.1988
T_{em}		505.9361	507.9833	512.9048	518.5809	527.6784
T_{cb}		362.2500	362.2484	362.2375	362.2482	362.2236
T_{ca}		363.1540	363.1500	363.1462	363.1568	363.1497
\dot{m}_{air}		18.0228	18.0725	18.1718	18.3174	18.5628
m_{air}		1.8022	1.8072	1.8171	1.8317	1.8562
λ		3.8479	3.8907	3.8991	3.8998	3.8631
p_{IVO}		169.6438	168.0804	167.3857	164.5102	162.7465
p_{IVC}		114.6138	114.7633	115.0373	115.2592	116.4997
p_{EVO}		224.0623	224.7561	229.2052	236.9178	244.2239
p_{EVC}		178.5535	177.1455	176.5846	174.5669	173.7357
m_{EVC}		0.4480	0.4438	0.4388	0.4307	0.4224
$x_{b,res}$		27.2906	26.9959	26.9389	26.9340	27.1855
$x_{b,IVC}$		5.4206	5.3051	5.2279	5.1242	5.0289
T_{EVC}		569.9658	570.8721	575.5024	579.6509	588.1826
T_{fc}		346.6537	346.5919	346.4711	346.1727	346.0864
T_{res}		327.5888	328.1407	330.3216	332.8197	336.6794 [
T_{IVC}		347.5436	347.5865	347.9651	348.2234	348.9232
T_a		491.7193	489.8685	489.5147	490.4355	490.5265
		486.6544	485.9364	485.9293	487.0716	486.6749
		489.1869	487.9025	487.7220	488.7536	488.6007
T_w		383.0655	383.0629	383.0693	383.0621	383.0684
k	IVC: 70°	1.4726	1.4673	1.4648	1.4664	1.4639
	70 : 50°	1.4027	1.4024	1.4051	1.4051	1.4043
m_{IVC}	IGL	2.2556	2.2582	2.2612	2.2638	2.2836
	IVC: 70°	2.2204	2.2308	2.2360	2.2403	2.2564
	70: 50°	2.2324	2.2401	2.2446	2.2483	2.2657
	70: 50°	2.2556	2.2582	2.2612	2.2638	2.2836
	70: 50°	2.2439	2.2491	2.2528	2.2560	2.2746
	Average	2.2416	2.2473	2.2512	2.2545	2.2728
m_{air}	IGL	1.8076	1.8145	1.8224	1.8331	1.8612
	IVC: 70°	1.7724	1.7870	1.7972	1.8096	1.8339
	70: 50°	1.7843	1.7963	1.8058	1.8176	1.8432
	70: 50°	1.8076	1.8145	1.8224	1.8331	1.8612
	70: 50°	1.7959	1.8054	1.8140	1.8253	1.8522
	Average	1.7936	1.8035	1.8124	1.8238	1.8503
$m_{air,err}$	IGL	0.2983	0.4038	0.2877	0.0800	0.2670
	IVC: 70°	-1.6525	-1.1171	-1.0955	-1.2058	-1.1995
	70: 50°	-0.9909	-0.5993	-0.6237	-0.7677	-0.6990
	70: 50°	0.2983	0.4038	0.2877	0.0801	0.2670
	70: 50°	-0.3497	-0.0998	-0.1697	-0.3453	-0.2179
	Average	-0.4793	-0.2017	-0.2627	-0.4317	-0.3165

Table B.10: Test 10- IVO:-324.7; IVC:-132.8; EVO:114.3; EVC:320.2

		cycle 1	cycle 2	cycle 3	cycle 4	cycle 5	cycle 6	cycle 7
Engine Speed		1200.0610	1200.0800	1200.0690	1200.0480	1200.0620	1200.0780	1200.0510
Engine Torque		363.9020	363.9183	363.6833	363.7011	363.5470	363.6043	363.4614
P_{im}		122.8459	123.2200	124.0640	125.5072	125.1671	127.0559	126.5945
P_{em}		117.4254	117.8535	118.2543	118.9909	118.8305	119.5046	119.3166
T_{im}		311.2487	311.4222	311.0497	310.8074	311.1595	310.9359	311.0090
T_{em}		578.1778	581.7678	586.4488	593.1799	589.5985	598.4582	593.5836
T_{cb}		361.6945	361.6500	361.6866	361.7251	361.7250	361.6962	361.6698
T_{ca}		363.1500	363.1413	363.1498	363.1500	363.1500	363.1540	363.1500
\dot{m}_{air}		19.5777	19.6727	19.9097	20.2452	20.1009	20.4948	20.3810
m_{air}		1.9577	1.9671	1.9909	2.0244	2.0100	2.0493	2.0380
λ		2.6417	2.6694	2.6903	2.7016	2.6896	2.6884	2.6855
p_{IVO}		160.3805	160.5347	160.1833	157.5430	158.5719	157.4856	159.4086
p_{IVC}		121.9128	122.4932	123.2343	124.7033	123.8735	126.2171	125.7754
p_{EVO}		284.0463	289.5356	293.6987	301.9067	291.8821	304.9410	296.3988
p_{EVC}		173.0444	172.6221	171.8001	170.7499	170.6611	170.2880	171.9298
m_{EVC}		0.3871	0.3844	0.3804	0.3750	0.3770	0.3714	0.3769
$x_{b,res}$		39.4350	39.0356	38.7403	38.5823	38.7504	38.7676	38.8084
$x_{b,IVC}$		6.4751	6.3419	6.1856	6.0041	6.0936	5.9024	6.0179
T_{EVC}		639.7019	642.6305	646.3818	651.6323	647.8844	656.1546	652.7514
T_{fc}		346.4946	346.6255	346.2133	345.8810	345.8273	345.6911	345.8766
T_{res}		359.6190	361.6817	362.8997	366.3073	363.2477	367.7761	366.0666
T_{IVC}		353.6718	354.0833	353.8281	353.9612	353.4396	353.8863	353.8983
T_a		495.9482	498.9817	498.5164	496.1523	496.4673	494.7892	496.0847
		493.1177	494.6497	494.6255	493.2305	494.1294	492.6641	493.3214
		494.5330	496.8157	496.5710	494.6913	495.2984	493.7266	494.7030
T_w		385.2209	385.2214	385.2187	385.2185	385.2171	385.2180	385.2160
k	IVC: 70°	1.4604	1.4672	1.4669	1.4599	1.4628	1.4564	1.4599
	70 : 50°	1.4043	1.3995	1.4003	1.4040	1.4042	1.4043	1.4028
m_{IVC}	IGL	2.3578	2.3663	2.3823	2.4097	2.3973	2.4395	2.4309
	IVC: 70°	2.3374	2.3351	2.3541	2.3882	2.3801	2.4235	2.4103
	70: 50°	2.3444	2.3457	2.3637	2.3956	2.3860	2.4290	2.4174
	70: 50°	2.3578	2.3663	2.3823	2.4097	2.3973	2.4395	2.4309
	70: 50°	2.3511	2.3560	2.3729	2.4026	2.3916	2.4342	2.4241
	Average	2.3497	2.3539	2.3711	2.4012	2.3904	2.4332	2.4227
m_{air}	IGL	1.9707	1.9818	2.0019	2.0347	2.0203	2.0681	2.0539
	IVC: 70°	1.9502	1.9507	1.9737	2.0132	2.0031	2.0521	2.0334
	70: 50°	1.9572	1.9613	1.9833	2.0206	2.0090	2.0576	2.0404
	70: 50°	1.9707	1.9818	2.0019	2.0347	2.0203	2.0681	2.0539
	70: 50°	1.9639	1.9715	1.9926	2.0276	2.0146	2.0628	2.0472
	Average	1.9625	1.9694	1.9907	2.0262	2.0135	2.0617	2.0458
$m_{air,err}$	IGL	0.6638	0.7471	0.5551	0.5091	0.5122	0.9144	0.7815
	IVC: 70°	-0.3811	-0.8364	-0.8612	-0.5568	-0.3409	0.1360	-0.2287
	70: 50°	-0.0235	-0.2972	-0.3788	-0.1919	-0.0495	0.4031	0.1171
	70: 50°	0.6638	0.7471	0.5551	0.5091	0.5122	0.9144	0.7815
	70: 50°	0.3192	0.2227	0.0863	0.1576	0.2307	0.6582	0.4484
	Average	0.2484	0.1166	-0.0087	0.0854	0.1729	0.6052	0.3800

Table B.11: Test 11- IVO:-324.7; IVC:-132.8; EVO:114.3; EVC:320.2

		cycle 1
Engine Speed		1800.0280
Engine Torque		319.8585
p_{im}		108.4183
p_{em}		112.8300
T_{im}		309.9792
T_{em}		650.9227
T_{cb}		361.3605
T_{ca}		363.2034
\dot{m}_{air}		26.1392
m_{air}		1.7426
λ		2.2035
p_{IVO}		189.9538
p_{IVC}		114.7839
p_{EVO}		283.5926
p_{EVC}		192.8096
m_{EVC}		0.3705
$x_{b,res}$		47.0400
$x_{b,IVC}$		8.1782
T_{EVC}		745.1835
T_{fc}		354.6927
T_{res}		389.7191
T_{IVC}		368.4801
T_a		533.5103
		524.4703
		528.9904
T_w		395.6091
k	IVC: 70°	1.5040
	70 : 50°	1.4062
m_{IVC}	IGL	2.1309
	IVC: 70° BTDC	2.0769
	70: 50° BTDC	2.0948
	70: 50° BTDC	2.1309
	70: 50° BTDC	2.1127
Average		2.1093
m_{air}	IGL	1.7605
	IVC: 70°	1.7065
	70: 50°	1.7244
	70: 50°	1.7605
	70: 50°	1.7423
Average		1.7388
$m_{air,err}$	IGL	1.0260
	IVC: 70°	-2.0731
	70: 50°	-1.0460
	70: 50°	1.0260
	70: 50°	-0.0189
Average		-0.0189

Table B.12: Test 12- IVO:-309.7; IVC:-117.8; EVO:99.3; EVC:305.2

		cycle 1	cycle 2	cycle 3	cycle 4	cycle 5
Engine Speed		1200.0660	1200.0800	1200.0550	1200.0670	1200.0420
Engine Torque		164.1016	163.7865	163.7869	163.3853	163.5047
P_{im}		116.3556	115.8138	114.9383	114.3424	114.1466
P_{em}		111.2568	111.0266	110.4394	110.0044	109.9249
T_{im}		321.1160	321.0110	320.9628	321.1239	321.2033
T_{em}		572.4804	571.8933	563.0869	557.6181	556.5243
T_{cb}		361.9739	362.0032	361.9583	361.9661	361.9477
T_{ca}		363.1554	363.1502	363.1497	363.1551	363.1502
\dot{m}_{air}		14.1876	14.0735	13.8942	13.7345	13.6609
m_{air}		1.4187	1.4073	1.3894	1.3734	1.3660
λ		2.8417	2.8646	2.8684	2.8468	2.8039
P_{IVO}		132.8442	129.7431	130.0395	132.2266	133.0680
P_{IVC}		116.0474	115.3986	114.0645	114.1558	113.6979
P_{EVO}		264.8685	272.5199	263.8423	260.5437	258.1566
P_{EVC}		152.0443	149.8843	150.2202	151.3525	151.1411
m_{EVC}		0.5610	0.5553	0.5641	0.5721	0.5726
$x_{b,res}$		36.7252	36.4391	36.3909	36.6608	37.2081
$x_{b,IVC}$		10.3596	10.2327	10.4792	10.6999	10.8977
T_{EVC}		621.4080	618.8217	610.6012	606.5356	605.2302
T_{fc}		359.9937	359.8701	359.9731	360.6534	360.5518
T_{res}		334.1984	334.7211	332.1058	330.6904	329.4897
T_{IVC}		361.9051	361.9174	361.1595	361.1825	360.7154
T_a		489.6388	492.1394	491.7720	494.0110	493.8491
		487.8142	489.4807	489.0880	489.7162	489.7563
		488.7265	490.8100	490.4300	491.8636	491.8027
T_w		383.0717	383.0685	383.0681	383.0640	383.0648
k	IVC: 70°	1.4751	1.4831	1.4852	1.4923	1.4938
	70 : 50° BTDC	1.4210	1.4177	1.4231	1.4137	1.4169
m_{IVC}	IGL	1.9888	1.9776	1.9589	1.9603	1.9550
	IVC: 70°	1.9766	1.9601	1.9414	1.9325	1.9286
	70: 50°	1.9814	1.9669	1.9482	1.9433	1.9388
	70: 50°	1.9888	1.9776	1.9589	1.9603	1.9550
	70: 50°	1.9851	1.9722	1.9535	1.9518	1.9469
	Average	1.9841	1.9709	1.9522	1.9497	1.9449
m_{air}	IGL	1.4278	1.4223	1.3948	1.3882	1.3824
	IVC: 70°	1.4156	1.4048	1.3773	1.3604	1.3560
	70: 50°	1.4204	1.4116	1.3841	1.3711	1.3662
	70: 50°	1.4278	1.4223	1.3948	1.3882	1.3824
	70: 50°	1.4241	1.4169	1.3894	1.3796	1.3743
	Average	1.4231	1.4156	1.3881	1.3775	1.3723
$m_{air,err}$	IGL	0.6424	1.0662	0.3910	1.0786	1.1995
	IVC: 70°	-0.2157	-0.1768	-0.8679	-0.9457	-0.7342
	70: 50°	0.1200	0.3070	-0.3785	-0.1623	0.0134
	70: 50°	0.6424	1.0662	0.3910	1.0786	1.1995
	70: 50°	0.3807	0.6856	0.0052	0.4554	0.6040
	Average	0.3140	0.5897	-0.0918	0.3009	0.4564

Bibliography

- [1] Ivan Arsie, Cesare Pianese, and G Rizzo. Estimation of air-fuel ratio and cylinder wall temperature from pressure cycle in si automotive engines. In *Proc. of IFAC Workshop on "Advances in Automatic Control"*, Mohican State Park, Ohio, 1998. Cited on page 21.
- [2] Ivan Arsie, Rocco Di Leo, Cesare Pianese, and Matteo De Cesare. Estimation of in-cylinder mass and afr by cylinder pressure measurement in automotive diesel engines. *IFAC Proceedings Volumes*, 47(3):11836–11841, 2014. Cited on pages 2, 13, 14, 34, 35, and 36.
- [3] Ivan Arsie, Rocco Di Leo, Stefano Falco, Cesare Pianese, and Matteo De Cesare. Estimation of the engine thermal state by in-cylinder pressure measurement in automotive diesel engines. Technical report, SAE Technical Paper, 2015. Cited on pages v, xii, 21, 22, and 23.
- [4] Michael FJ Brunt and Christopher R Pond. Evaluation of techniques for absolute cylinder pressure correction. Technical report, SAE technical paper, 1997. Cited on pages 27 and 28.
- [5] Ritchie Daniel, Chongming Wang, Hongming Xu, and Guohong Tian. Effects of combustion phasing, injection timing, relative air-fuel ratio and variable valve timing on si engine performance and emissions using 2, 5-dimethylfuran. *SAE International Journal of Fuels and Lubricants*, 5(2012-01-1285):855–866, 2012. Cited on page 27.
- [6] JM Desantes, J Galindo, C Guardiola, and V Dolz. Air mass flow estimation in turbocharged diesel engines from in-cylinder pressure measurement. *Experimental Thermal and Fluid Science*, 34(1):37–47, 2010. Cited on pages 11, 12, 13, and 14.
- [7] D Descieux and M Feidt. One zone thermodynamic model simulation of an ignition compression engine. *Applied Thermal Engineering*, 27(8):1457–1466, 2007. Cited on page 29.
- [8] Lars Eriksson and Lars Nielsen. *Modeling and Control of Engines and Drivelines*. John Wiley & Sons, 2014. Cited on pages 1, 5, 6, 7, 8, 9, 10, and 27.

- [9] Lars Eriksson and Andreas Thomasson. Cylinder state estimation from measured cylinder pressure traces- a survey. 2016. Cited on pages 11, 12, and 13.
- [10] P Giansetti, G Colin, Y Chamailard, and P Higelin. Two observers for in-cylinder mass estimation using cylinder pressure measurements. *IFAC Proceedings Volumes*, 40(10):219–226, 2007. Cited on pages v, 2, 13, 15, 16, and 69.
- [11] C Guardiola, V Triantopoulos, P Bares, S Bohac, and A Stefanopoulou. Simultaneous estimation of intake and residual mass using in-cylinder pressure in an engine with negative valve overlap. *IFAC-PapersOnLine*, 49(11): 461–468, 2016. Cited on page 16.
- [12] John B. Heywood. *Internal Combustion Engine Fundamentals*. McGraw-Hill, 1988. Cited on pages xii, 7, 9, 10, 17, 18, 20, 30, and 31.
- [13] H Hong, G B Parvate-Patil, and B Gordon. Review and analysis of variable valve timing strategies—eight ways to approach. *Proceedings of the Institution of Mechanical Engineers, Part D: Journal of Automobile Engineering*, 218(10):1179–1200, 2004. doi: 10.1177/095440700421801013. URL <http://dx.doi.org/10.1177/095440700421801013>. Cited on page 27.
- [14] Jack PC Kleijnen. Sensitivity analysis and related analyses: a review of some statistical techniques. *Journal of statistical computation and simulation*, 57(1-4):111–142, 1997. Cited on page 59.
- [15] Marcus Klein. A specific heat ratio model and compression ratio estimation. 2004. Cited on page 28.
- [16] Kangyoon Lee, Minsu Kwon, Myoungho Sunwoo, and Maru Yoon. An in-cylinder pressure referencing method based on a variable polytropic coefficient. Technical report, SAE Technical Paper, 2007. Cited on pages 27 and 28.
- [17] T Leroy, G Alix, J Chauvin, A Duparchy, and F Le Berr. Modeling fresh air charge and residual gas fraction on a dual independent variable valve timing si engine. *SAE International Journal of Engines*, 1(2008-01-0983): 627–635, 2008. Cited on pages xii and 38.
- [18] Mohand Said Lounici, Khaled Loubar, Mourad Balistrout, and Mohand Tazerout. Investigation on heat transfer evaluation for a more efficient two-zone combustion model in the case of natural gas si engines. *Applied Thermal Engineering*, 31(2):319–328, 2011. Cited on pages 17, 19, 20, and 33.
- [19] Frederic A Matekunas. Engine combustion control with fuel balancing by pressure ratio management, 1986. US Patent 4,621,603. Cited on page 27.
- [20] Frederic A Matekunas. Engine combustion control with dilution flow by pressure ratio management, 1986. US Patent 4,624,229. Cited on page 27.

-
- [21] E Ollivier. *Contribution to the characterization of heat transfer in spark ignition engines, Application to knock detection*. PhD thesis, Ph. D. thesis, ENSTIM de Nantes, France, 2006. Cited on page 17.
- [22] Andrea Saltelli, Marco Ratto, Terry Andres, Francesca Campolongo, Jessica Cariboni, Debora Gatelli, Michaela Saisana, and Stefano Tarantola. *Global sensitivity analysis: the primer*. John Wiley & Sons, 2008. Cited on page 59.
- [23] M.S. Silberberg. *Principles of general chemistry*. McGraw-Hill Higher Education, 2007. ISBN 9780073107202. Cited on page 29.
- [24] Jeremy Worm. An evaluation of several methods for calculating transient trapped air mass with emphasis on the “delta p” approach. Technical report, SAE Technical Paper, 2005. Cited on pages 11, 14, and 17.
- [25] Gerhard Woschni. A universally applicable equation for the instantaneous heat transfer coefficient in the internal combustion engine. Technical report, SAE Technical paper, 1967. Cited on pages 19 and 20.